Geoscience Frontiers 14 (2023) 101612

HOSTED BY

Contents lists available at ScienceDirect

Geoscience Frontiers

journal homepage: www.elsevier.com/locate/gsf

Research Paper

Large earthquakes along slow converging plate margins: Calabrian Arc paleoseismicity based on the submarine turbidite record

A. Polonia [a,*], R. Melis [b], P. Galli [c], E. Colizza [b], D.D. Insinga [a], L. Gasperini [a]

[a] Istituto di Scienze Marine (ISMAR-CNR), Consiglio Nazionale delle Ricerche, Area della Ricerca di Bologna, Italy
[b] Dipartimento di Matematica e Geoscienze, Università degli Studi di Trieste, Italy
[c] Presidenza del Consiglio dei Ministri, Dipartimento della Protezione Civile, Servizio Rischio Sismico - Roma, Italy

ARTICLE INFO

Article history:
Received 20 June 2022
Revised 29 December 2022
Accepted 5 April 2023
Available online 11 April 2023
Handling Editor: Masaki Yoshida

Keywords:
Calabrian Arc
Earthquakes
Seismic shaking
Sedimentation
Seismo-turbidites

ABSTRACT

The Calabrian Arc subduction-rollback system hosts seismogenic faults capable of generating earthquakes exceeding magnitude 7. Since earthquakes are the result of long-term geodynamic processes, documenting seismic activity during a sufficiently long time interval is of fundamental importance for hazard scenarios. Instrumental and historical data provide critical information on seismogenesis, but they cover time periods shorter than the recurrence times of large earthquakes, especially in areas with low deformation rates such as Calabria. If onshore paleoseismological studies are fundamental to compile earthquake catalogs, they are sometime affected by the relatively poor continuity of sedimentation in the subaerial environment.

In this study we applied the paleoseismological approach to the submarine environment to reconstruct the record of high-energy sedimentary events triggered by seismic activity. We analyzed three gravity cores collected in disconnected sedimentary basins to reconstruct resedimentation processes during the Holocene, integrating inland information for a better assessment of tectonic activity and seismogenesis. Multiproxy analyses of the sedimentary record constrained by radiometric dating allowed reconstructing event stratigraphy and linking resedimented deposits to specific earthquakes.

Onshore and offshore data allow to identify large-magnitude earthquakes in the central Calabrian Arc subduction system during the Holocene, with inferred epicenters located either along normal faults onshore and/or related to the slab dynamics. The turbidite record reveals 20 major events during the last 10 ka, with sources including crustal faults in Calabria (i.e. Lakes, Rossano and Cittanova faults). Analyses of sediment samples and high-resolution seismic reflection images allowed identification of different types of resedimented deposits during the last 30–50 ka. The basin-wide occurrence of three megaturbidites/homogenites suggests they are related to megatsunamis sourced by far field earthquakes along the Hellenic Arc. Megaturbidites with a more limited spatial extent are interpreted as subduction-type events in the Calabrian Arc, while thinner seismo-turbidites record the activity of crustal structures including faults onshore. Results suggest a recurrence time of 2–3 ka for major Calabrian Arc events that needs to be considered for a reliable hazard assessment in the Mediterranean region.

1. Introduction

The Calabrian Arc (CA) is a subduction and rollback system populated by seismogenic structures capable of generating earthquakes exceeding magnitude 6.7, as those that occurred in March-June 1638, February-March 1783, September 1905, and December 1908. As the physiography of the Mediterranean basin is characterized by narrow continental shelves, steep slopes and uplifting coastal mountain ranges, it produces high sediment discharge in the submarine environment, increasing the susceptibility of slope failures and sediment remobilization during seismic shaking (Polonia et al., 2013a). This is the main reason why major earthquakes in the CA are often associated with tsunamis (Tinti et al., 2004) whose triggering mechanism can be ascribed both to earthquake seafloor rupture and to submarine landslides (Schambach et al., 2020). For instance, in Calabria, this is historically documented in the March 1638 earthquake, in the February-March 1783, March 1832, April 1836, September 1905

* Corresponding author.
E-mail address: alina.polonia@cnr.it (A. Polonia).

https://doi.org/10.1016/j.gsf.2023.101612

events and in the catastrophic earthquake and tsunami of December 28, 1908.

The coastal areas of southern Italy are also threatened by far field events along the Hellenic Arc that are capable of generating trans-Mediterranean tsunamis (Tinti et al., 2005; Lorito et al., 2008; Shaw et al., 2008). For instance, the tsunami related to the CE 365 Crete earthquake affected the Ionian and Adriatic coasts (i.e., Chronicon of Jerome, 4th century: "*There was an earthquake all over the World, the sea broke on the shore killing the inhabitants of Sicily and of many other islands*". Jerome, Life of St. Hilarion, 4th century: "*Then there was an earthquake all over the World…and the sea went out of its borders…ships were dragged on steeps mountains remaining suspended. And when the inhabitants of Epidaurus* (former Ragusa Vecchia, now Cavtat in Croatia) *saw this, they were afraid that the sea waves as high as mountains would crash down the coast, as it was happening, and destroy entirely their town*"). Marine geological data documented that this tsunami produced giant slope failures along the continental margins of eastern Sicily and Calabria (Polonia et al., 2013b, 2022; San Pedro et al., 2017).

Although instrumental and historical data can provide critical information for seismic hazard, they cover time periods shorter than the recurrence times of large earthquakes, especially in areas with low deformation rates, such as the Mediterranean region (Galli, 2020). On the other hand, paleoseismological studies may aid in completing the seismic catalogs (Galli et al., 2008). Unfortunately, trench studies, the most common applied paleoseismological method in the subaerial environment, are sometimes affected by poor continuity of sedimentation. A paleoseismological approach to the marine record has the potential of reconstructing a more complete record of high-energy sedimentary events triggered by seismic activity, during long time intervals which may include a number of seismic cycles (McHugh et al., 2006; Goldfinger, 2011). This approach was already tested in the submarine CA region offshore eastern Sicily where major historical earthquakes triggered the deposition of decimetric thick seismoturbidites (STs) (Polonia et al., 2013a, 2017a, 2021a, 2021b). Resedimented beds were used to study the interplay between earthquakes and sedimentation during the deposition of sapropel S1 (Polonia et al., 2015), an organic carbon-rich lower Holocene marker bed in the Eastern Mediterranean Sea (6.0 and 10.2 ka cal BP) whose peculiar color, composition, geochemistry and age, make it a key bed where turbidites are easily recognizable within the background dark pelagic sedimentation.

Paleoseismic trenching in the Calabria inland allowed to discover some of the seismogenic sources of major earthquakes, such as those of 5 and 7 February 1783 (Mw 7 and Mw 6.7, respectively), or 9 June 1638 (Mw 6.7) as well as their numerous predecessors, either mentioned in the historical literature or having occurred before, in the Holocene (Galli and Bosi, 2002, 2003; Galli and Scionti, 2006; Galli and Peronace, 2015). However, we still ignore the faults that generated the two strongest Calabria earthquakes, namely the 1905 (Ms 7.5; Margottini et al., 1993) and 1908 (Mw 7.1; Rovida et al., 2022) events, both occurred offshore the western and southern coast of Calabria, respectively (Michelini et al., 2006; Galli and Molin, 2007).

In this work, we analyzed turbidites as likely records of past earthquakes and we present an improved review of large-magnitude Calabrian historical earthquakes obtained by integrating paleoseismological data onshore with a multiproxy analysis of three gravity cores collected in sedimentary basins offshore southeast Calabria (CALA-10, CALA-15 and CALA-20 in Fig. 1). We then propose an extension of the paleo-earthquake record to prehistorical times (30–50 ka) by combining marine geological and geophysical data.

2. Tectonic setting

The study area is part of the CA accretionary wedge where regional deformation is driven by the slow convergence of Africa and Europe (4 mm/yr) in combination with the Ionian slab rollback (Fig. 1). The migrating trench drives the entire accretionary wedge outward with major differences between the eastern lobe (EL) offshore Calabria that is colliding with the Mediterranean Ridge, and the western lobe (WL) offshore Sicily, free to spread into the abyssal plain of the Ionian Sea. Extensional faulting and basin formation offshore Sicily are an expression of this spreading as well as incipient rifting processes that produce a collapse of the subduction complex (Polonia et al., 2016b, 2017b). On the other hand, the EL shows a more elevated accretionary wedge, 1000–1500 m shallower than the corresponding WL, steeper topographic slopes, a deeper basal detachment depth (about 4 km deeper relative to the WL) and thrust faults involving the basement (i.e. thick-skinned tectonics; Bortoluzzi et al., 2017). The WL corresponds to areas where the slab is already detached, while the EL corresponds to the region of the CA where local earthquake tomographic maps image a continuous slab penetrating into the mantle (Wortel and Spakman, 2000; Faccenna et al., 2007; Neri et al., 2009, 2012) together with a well-defined Wadati-Benioff zone (Wortel and Spakman, 2000) marked by earthquakes down to nearly 500 km depth (Selvaggi and Chiarabba, 1995). In this area, geodetic measurements suggest the outward motion of Calabria relative to Apulia (GPS rate of 2 mm/yr; D'Agostino et al., 2008) with shortening accommodated in the accretionary wedge (Polonia et al., 2011). Furthermore, tomographic imaging has shown that the deep (lithosphere-upper mantle) structure in the Calabrian-Sicily region has the characteristics of a STEP setting (Subduction-Transform Edge Propagator; Govers and Wortel, 2005) with distinct edges that laterally bound the narrow CA both northeast and southwest of the EL (Neri et al., 2012; Maesano et al., 2017). These are loci of lithospheric tearing resulting from the subduction of the (retreating) Calabria slab while adjacent parts (Apulia, Sicily) remain at the earth surface. Margin segmentation occurs along inherited transform faults bounding crustal blocks with different mechanical behavior similarly to other active margins (Polonia et al., 1999).

The accretionary wedge in the study region shows a rough morphology with ridges and troughs, steep scarps and a depressed area (intermediate depressions of Rossi and Sartori, 1981) that may be considered as the shallow expression of out-of-sequence thrusts and splay fault activity. The intermediate depressions are bounded to the NW by the Calabria Escarpment, a prominent transpressive feature segmenting longitudinally the subduction complex and triggering mud diapirism (Panieri et al., 2013). Inwards of the Calabria Escarpment, a rather flat area is imaged (i.e. the inner plateau). While crustal shortening is taken up in the accretionary wedge, transtensive deformation accounts for margin segmentation along transverse lithospheric faults controlling the formation of forearc basins (Fig. 1) (Capozzi et al., 2012). Our cores were collected in the intermediate depressions and in a deep sedimentary basin developed in the inner plateau and inner accretionary wedge of the CA Eastern Lobe (Fig. 1).

Active tectonics in Calabria is due to normal or oblique faults bounding the Plio-Quaternary basins of northern Calabria, Crati Valley and Catanzaro Straits (central Calabria), and Mesima-Gioia Tauro Plain (southern Calabria), beside others in Sila Mts and in the Messina Strait (Fig. 2). Several faults, investigated through paleoseismological analyses, revealed a Late Pleistocene-Holocene activity; they are the faults of Mt. Pollino (Ferreli et al., 2002), Rossano (Galli et al., 2010), Lakes (Galli and Bosi, 2003; Galli and Scionti, 2006), Serre (Galli et al., 2007), and Cittanova

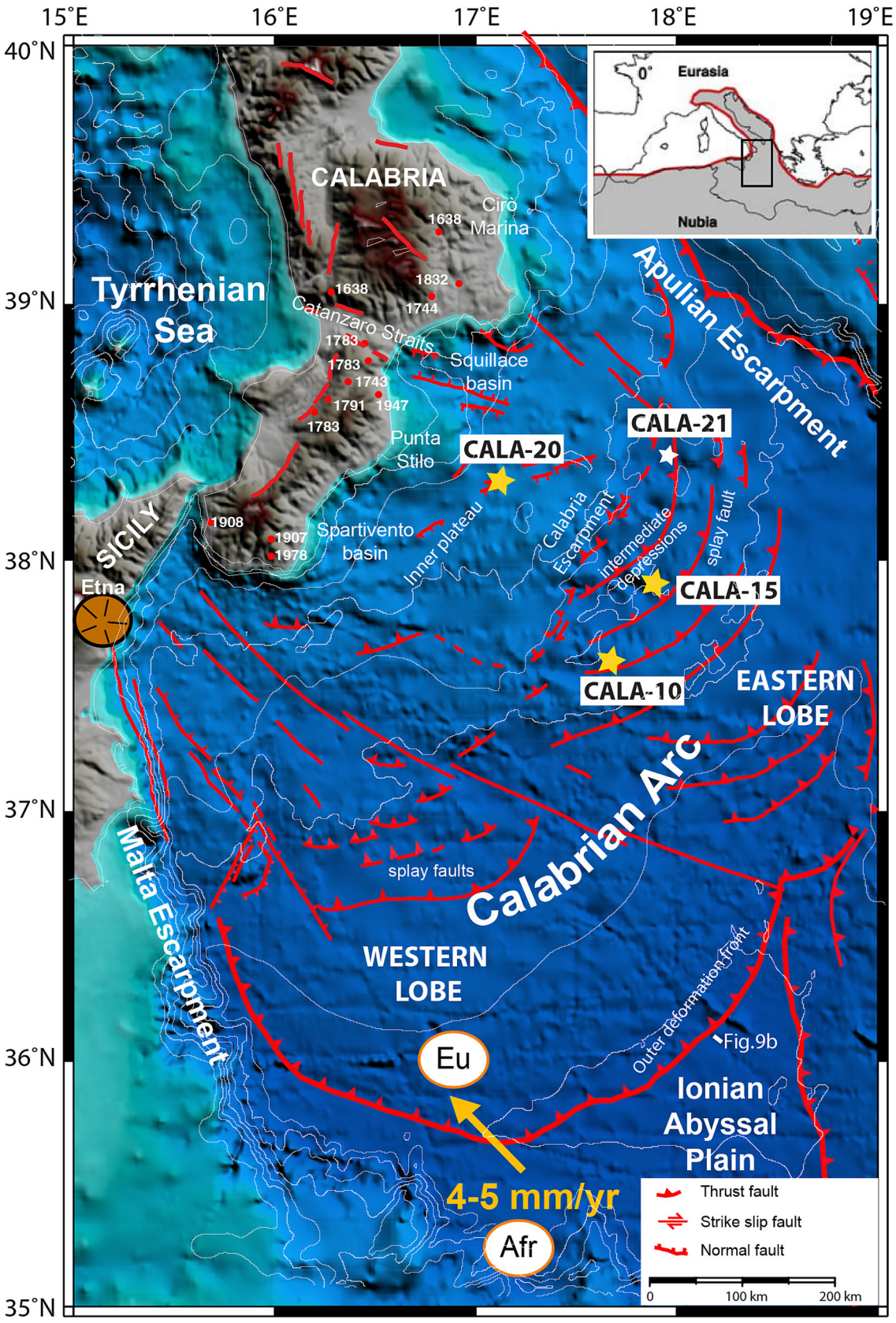

Fig. 1. Geodynamic setting of the study area and structural map of the Calabrian Arc subduction system in the Ionian Sea as derived from the interpretation of available seismic data (Polonia et al., 2011) integrated with GEBCO bathymetry data. Yellow arrow indicates Europe (Eu) and Africa (Afr) slip vector in the Afr reference frame. Note the presence of seismogenic faults segmenting the margin both across and along strike (red lines). Yellow stars indicate the cores described in this study (cores CALA-10, 15, 20) and the location of Chirp profiles collected on the coring site and shown in Fig. 3; white star indicates CALA 21 (Polonia et al., 2015). Epicentres of historical earthquakes (Rovida et al., 2022) are indicated by red circles.

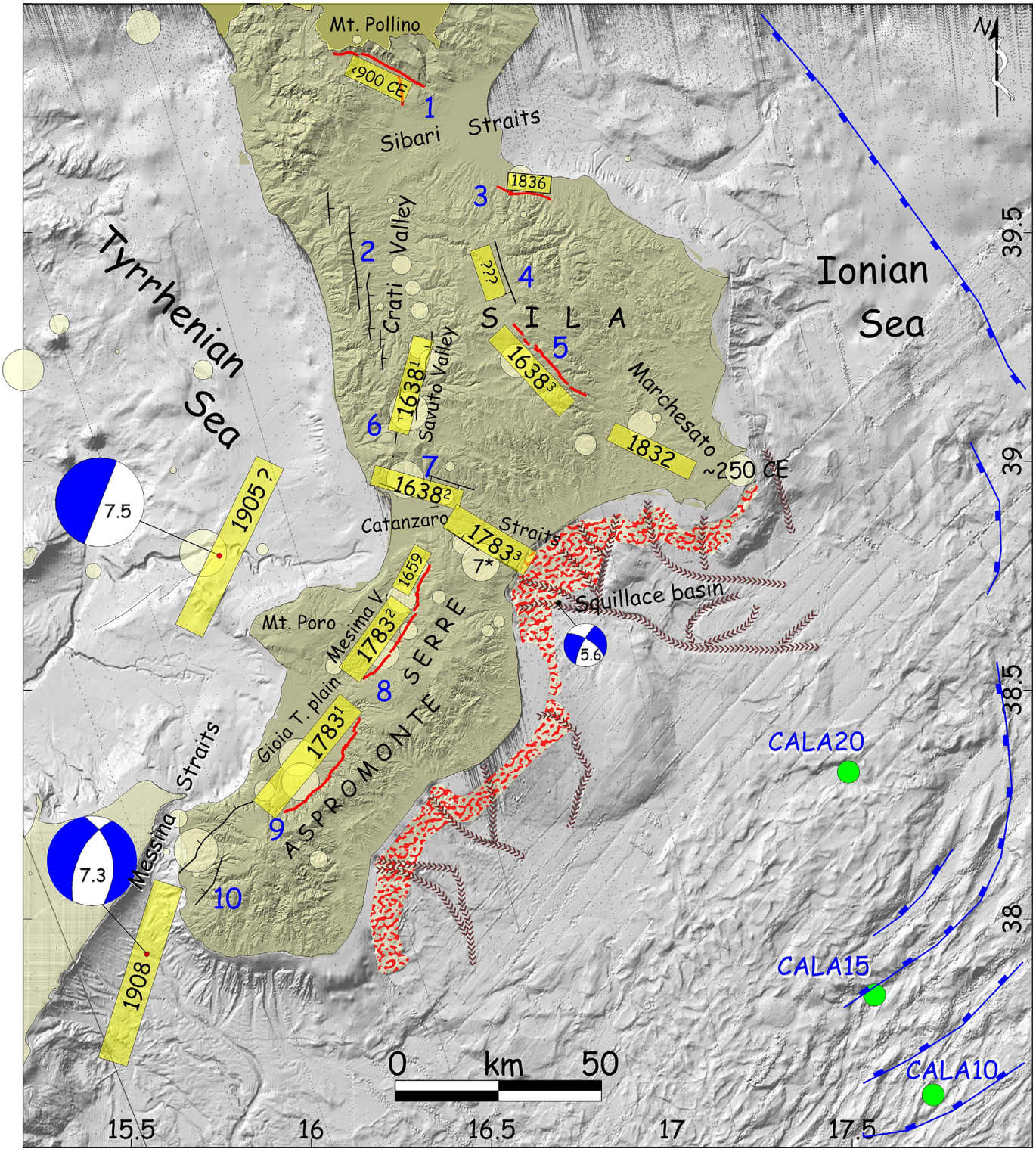

Fig. 2. Shaded relief map of Calabria showing the primary seismogenic faults (1, Mt. Pollino fault; 2, W-Crati fault system; 3, Rossano fault; 4, Cecita fault; 5, Lakes fault; 6, Savuto fault system (Piano Lago-Decollatura fault); 7, Catanzaro Straits faults: Feroleto-Sant'Eufemia fault and 7*, Stallettì-Maida fault system; 8, Serre fault system; 9, Cittanova fault; 10, Reggio Calabria fault system) and the possible source of the main earthquakes (yellow boxes are the surficial projection of the seismogenic structure at depth). Red bold lines are the faults investigated through paleoseismological analyses, with the date of the last, certain earthquake rupture. Thin lines are Quaternary faults, likely associated with historical earthquake. Red areas along the Ionian coast of Calabria match the potential turbidites source region. The landward limit of sediment source areas follows the retrogressive margin trend on the shelf. The main morpho-sedimentary features (canyon axis in brown) are taken from Ceramicola et al. (2021).

(Galli and Bosi, 2002; Galli and Peronace, 2015). To date, despite documented historical and instrumental low-moderate seismicity, we have no reliable geological data concerning deformation of Upper Pleistocene deposits along the Crati, Catanzaro Straits, Marchesato, and Reggio Calabria fault systems (e.g. in Galli et al., 2007).

3. Seismicity and paleoseismicity

The seismicity of the Calabrian peninsula is one of the strongest in the Mediterranean region, both in terms of maximum magnitude and frequency of the main events (at least 25 M > 6 earthquakes since 91 BCE between the Messina Strait and the Crati basin; Rovida et al., 2022). However, beyond sparse and uncertain reports from the 16th century, our knowledge of regional seismicity starts only with the onset of the 17th century (Table 1), when several 5.5 ≤ Mw ≤ 6.8 events struck central and southern Calabria (Scionti et al., 2006). These include the triplet between 27 and 28 March 1638 (Mw 6.8–6.6, Savuto valley and western Catanzaro Straits; Galli and Bosi, 2003), followed on June 9 by another mainshock in Sila Mts (Mw 6.7; Galli and Scionti, 2006), and on November 5, 1659 by another destructive event in the northern Serre Ridge (Mw 6.6; Galli et al., 2007). After a century of seismic silence, two strong earthquakes in 1743 (Mw 5.9) and 1744 (Mw 6.2) hit southern and central Calabria, respectively (Scionti et al., 2006), preceding by 40 years the most catastrophic seismic sequence that ever occurred in Europe. This started on February 5, 1783 with a Mw 7.0 earthquake that razed to the ground all villages of the Gioia Tauro Plain, followed on February 7 by a Mw 6.6 shock in the adjacent Mesima Valley, and another Mw 7.0 event that struck the eastern Catanzaro Strait on March 28 (ENEL, 1986). This sequence killed around 35,000 people, destroying more than 150 villages, and causing hundreds of giant landslides (Cotecchia et al., 1986). After another century of silence, a Mw 6.1 event hit again in 1894 the Gioia Tauro Plain, preceding by few years the two strongest events of the twentieth century, 1905 and 1908 earthquakes of Mw > 7.

95% of the seismic moment release in the past millennium occurred between the disruptive earthquakes of March 1638 and those of 1905 and 1908. Considering that the average time-recurrence for characteristic earthquakes on each fault (~1.2–3.1 ka; Galli, 2020) is much longer than the period of completeness of the Calabrian catalogue (~0.5 ka for M > 6; GdL, 2004), the latter missed most of the ancient predecessors of the major events that struck Calabria. Therefore, paleoseismic investigations in Calabria have been determinant both in defining the faults responsible for the major historical events and in unearthing paleo-earthquakes dating back to times not or poorly covered by written accounts.

In particular, trenching across the previously unknown Lakes fault (Sila Mts, central Calabria), allowed recognizing the June 1638, Mw 6.8 earthquake, in addition to three unreported predecessors in the 7th century CE, in the early 1st millennium BCE, and in the early 2nd millennium BCE, respectively. In turn, trenching across the Cittanova fault (Aspromonte Range, southern Calabria), permitted to recognize the catastrophic, February 5, 1783 Mw 7.0 earthquake, and four predecessors. The first one was related to an event that occurred just before 374 CE, year provided by an epigraph mentioning the Reggio Calabria earthquake (Galli and Bosi, 2002). The second occurred in the early 4th millennium BCE, the third in the late 9th millennium BCE and the fourth in the early 11th millennium BCE. Other trenches opened across the adjacent Serre fault indicated the effects of the February 7, 1783 Mw 6.7 earthquake, and of other undetermined faulting episodes in the Holocene. Finally, the trenches across the Rossano fault (northern Calabria) identified the earthquakes of 1836 (Mw 6.3) and a possible predecessor in 951 CE.

4. Methods

To gather information on sediment remobilization processes, we used a multidisciplinary approach involving geochemical and physical analyses of sediment samples collected in separate basins. Gravity cores (CALA-10, CALA-15 and CALA-20) were collected during the CALAMARE cruise carried out on board of R/V Urania in 2008. Parameters, such as grain-size, magnetic susceptibility, and geochemical elemental data were acquired and integrated with micropaleontological and stratigraphic analyses, to unravel the relationships between sediment composition, provenance, sediment structures and, ultimately, sedimentary depositional processes in core CALA-20. Cores CALA-10 and -15 were instead analyzed visually for core correlation. Radiometric dating was performed in all cores.

Grain-size analyses were carried out on 166 samples with a varying sampling rate (1–6 cm) depending on visual characteristics. Sediment textures were analysed through a particle-counter laser MALVERN Mastersizer 2000 (Hydro 2000S), for size ranges from 0.02 to 2000 μm fraction. Sediment samples were treated with 20 vol hydrogen peroxide solution for 48 h. Results were classified according to Friedman and Sanders (1978) grain-size scale and are presented as % in sand, silt, clay and mean diameter (Mz) determined according to Folk and Ward (1957) and expressed in ϕ.

Table 1
Parametric catalogue of the main earthquakes (Mw > 6.0) occurred in the Calabria area in the past two millennia (Galli and Bosi, 2002, 2003; Scionti and Galli, 2004; Vannucci and Gasperini, 2004; Galli and Scionti, 2006; Michelini et al., 2006; Galli and Molin, 2007; Galli et al., 2010; Rovida et al., 2022).

Date	Io	Mw	Latitude	Longitude	Epicentral Area
~250	10.0	6.5	38.99	17.18	Cape Colonna
<374	11.0	7.0	38.36	15.99	Gioia Tauro plain
951	9.5	6.3	39.62	16.58	Rossano
1184 05 24	9.0	6.7	39.40	16.19	Norther Calabria
1638 03 27	11.0	6.8	39.11	16.27	Savuto Valley
1638 03 28	9.5	6.6	38.68	16.23	Serre north
1638 03 28	11.0	6.9	38.96	16.26	Western Catanzaro Strait
1638 06 09	10.0	6.7	39.22	16.57	Sila Grande east
1659 11 05	10.0	6.5	38.71	16.54	Serre north
1783 02 05	11.0	7.0	38.36	15.99	Gioia Tauro plain
1783 02 07	10.5	6.6	38.63	16.19	Serre south
1783 03 28	11.0	7.0	38.83	16.59	Eastern Catanzaro Strait
1832 03 08	10.0	6.6	39.08	16.92	Cutro
1836 04 25	9.5	6.3	39.62	16.58	Rossano
1854 02 12	10.0	6.3	39.26	16.30	Southern Crati Valley
1870 10 04	9.5	6.2	39.22	16.33	Southern Crati Valley
1894 11 16	9.0	6.1	38.29	15.87	Gioia Tauro plain
1905 09 08	10.5	7.4	38.80	15.70	Capo Vaticano offshore
1908 12 28	11.0	7.1	37.95	15.72	Messina Strait
1947 05 11	8.0	5.7	38.65	16.80	Squillace offshore

High-resolution magnetic susceptibility (MS) logs were acquired with a *Bartington*, model MS2, equipped with a 100 mm loop sensor at sampling intervals of 5 mm.

Geochemical data of core CALA-20 were collected by using an *Avaatech* XRF-CS at CNR-ISMAR under three different settings, 10 kV with 10 s measuring time (Al, Si, P, S, Cl, K, Ca, Ti, Cr, Mn, Fe, Rh, Ba), 30 kV with 20 s measuring time (Ni, Cu, Zn, Ga, Br, Rb, Sr, Y, Zr, Nb, Mo, Pb, Bi) and 50 kV with 30 s measuring time (Ag, Cd, Sn, Te, Ba). Measurements were performed with a step size of 1 cm along the cores. Since the main purposes of this work are to reconstruct depositional processes, to discriminate between different sediment sources and travelling paths, and to assess diagenetic processes, we selected diagnostic elemental ratios which traditionally track detrital alumino-silicates (e.g. Zr, Al, Fe, Ti), carbonates (e.g. mostly biogenic; Ca and Sr), lithogenic/detrital origin or/and paleoproductivity (e.g. Ba), diagenesis overprint (e.g. redox-sensitive elements: Fe, Mn, and S) and porosity or interstitial water content (S) (Chester, 2000).

Radiometric dating: accelerator mass spectrometry (AMS) radiocarbon dating of handpicked planktonic foraminifera was performed. We selected samples in the hemipelagic units (Table 2), some centimetres above the turbidites to avoid reworked tests possibly occurring close to the base of the turbidite. About 5–6 mg of specimens (mixed or monospecific when possible) > 125 μm in size from 1-cm thick samples were studied. Nine, eight and two samples were radiometrically dated in cores CALA-20, CALA-10 and CALA-15 respectively (Table 2). One level in core CALA-10 was dated also using the pteropod *Cavolinia* (Polonia et al., 2016a). The AMS analyses were performed at the Poznań Radiocarbon Laboratory - Foundation of the Adam Mickiewicz University (Poland).

The first step to reconstruct the turbidite event chronology was to calibrate the ^{14}C ages of the hemipelagic sediment samples using the MARINE20 calibration curve (Heaton et al., 2020) in CALIB Rev. 8.2 programme (Stuiver and Reimer, 1993). We decided not to apply a marine reservoir correction because of the lack of local data and the great dispersion of ΔR values in the surrounding region.

Age modelling: Since the samples of hemipelagic sediments are located a few cm above the top of the turbidite, it was necessary to interpolate the ages of the calibrated samples to estimate the age of each single turbidite. For this purpose, we reconstructed the deposition rate from two successive radiometric dates in the hemipelagic sequence. Moreover, given the uncertainty of individual calibrated radiocarbon determinations, we used information about the deposition process to refine our chronologies and provide an interpolation between dated levels that takes into account the error propagation. The age model is built using the P_Sequence (a Bayesian model of deposition from the computer program OxCal 4.1 that assumes sedimentation as a random process following a Poisson law (Bronk Ramsey, 2008)). The input parameters to generate the P_Sequence model are the uncalibrated ^{14}C ages and

Table 2
AMS radiometric data (uncalibrated ages) performed on cores CALA-20, CALA-10 and CALA-15, with their corresponding depth in the cores. Numbers in brackets in column 6 represent median probability.

1 Core name and water depth	2 Sample name and core depth (cm)	3 Type of sample	4 Lab. N.	5 ^{14}C measured age BP	6 Calibrated age (2σ) according to CALIB REV8.2 by Stuiver and Reimer (1993) ΔR = 0
CALA-20 (2050 m)	V 12–13 (8)	Foram	Poz-75426	730 ± 40	CE 1635–1950 (1765) [315–0 BP] *CE 1675–1840 (1 σ)*
	V 45–46 (41)	Foram	Poz-85768	1165 ± 30	CE 1270–1480 (1370) **[680–470 BP]**
	IV 39–40 (105)	Foram	Poz-75371	1710 ± 35	CE 700–990 (843) **[1250–960 BP]**
	IV 42–43 (108)	Foram	Poz-85769	1735 ± 30	CE 680–960 (816) **[1270–990 BP]**
	II 20–21 (286)	Foram	Poz-75181	3370 ± 70	BCE 1335–870 (−1100) **[3285–2820 BP]**
	II 90–91 (356)	Foram	Poz-75180	3990 ± 40	BCE 2045–1675 (−1866) **[3995–3625 BP]**
	I 80–81 (446)	Foram	Poz-75373	6240 ± 40	BCE 4695–4360 (−4528) **[6640–6305 BP]**
	I 86–87 (452)	Foram	Poz-75372	6850 ± 50	BCE 5380–5025 (−5218) **[7330–6975 BP]**
CALA-10 (2945 m)	IV 9.5–10.5 (10)	Foram	Poz-35779	1670 ± 35	CE 735–1030 (886) **[1215–920 BP]**
	II 8–9 (168)	Foram	Poz-35780	8430 ± 110	resedimented
	II 8–9 (168)	Cavolina	Poz-35782	7340 ± 50	resedimented
	II 18.3–19.3 (178)	Foram	Poz-35783	2700 ± 30	BCE 415 - CE 110 (−281) [**2365–2060 BP**]
	II 38–39.5 (198)	Foram	Poz-35784	3400 ± 35	BCE 1315–960 (−1140) [**3260–2905 BP**]
	II 70–71 (230)	Foram	Poz-37392	4415 ± 35	BCE 2610–2245 (−2431) [**4560–4195 BP**]
	II 87–88 (248)	Foram	Poz-35785	6010 ± 50	BCE 4460–4095 (−4289) [**6405–6045 BP**]
	I 60–61 (321)	Foram	Poz-35786	9030 ± 50	BCE 7800–7440 (−7594) [**9750–9390 BP**]
CALA-15 (2930 m)	IV 13.5 (13.5)	Foram	Poz-34940	700 ± 30	CE 1675–1950 (1793) **[275–0 BP]**
	IV 25.3 (25.3)	Foram	Poz-34941	1370 ± 90	CE 990–1395 (1187) **[960–555 BP]**

respective ΔR with their corresponding corrected depths. The regularity of sedimentation is determined by the k parameter with the higher values of k reflecting smaller variations in sedimentation rate (Bronk Ramsey, 2008). We chose k = 3.0 because we assumed that hemipelagic sedimentation is rather constant during the last 10 ka in the study area. The model finally calculates the age of each corrected depth corresponding to a turbidite and generates the 95.4% probability age ranges (2σ).

Micropaleontological analyses of foraminiferal assemblages were performed to gather information about sediment origin. A total of 102 sediment samples (1 cm thick) were investigated for foraminiferal analysis with higher resolution (i.e. every cm) in the intervals with high sand content and every 10 cm in the other sections of the core. The entire fraction > 63 μm was routinely investigated. Foraminiferal benthic counts were performed considering only well-preserved specimens and data were reported as relative abundance and as densities (number of specimens/g of total sediment). Indicative species with typical bathymetric distributions (Table 3) were used to identify the water depth from which the sediments were entrained. Following their deep-water preference, the frequency of the foraminifers was grouped into categories as follows: inner shelf (infralittoral taxa), shelf (taxa living from the infralittoral to the circalittoral), outer shelf - bathyal (taxa living from about 200 to 1000 m) and bathyal (taxa living at depths greater than 1000 m) (Supplementary Material 1).

Tephrostratigraphic analysis was carried out in order to provide an additional geochronological constraint along the studied successions. Following the lithological description at the optical microscope, an aliquot of the total samples was mounted on epoxy resin and suitably polished to be characterized in terms of major element composition through SEM-EDS technique at the DiSTAR SEM laboratory (University of Naples Federico II). Glass analyses were obtained through procedures described in Totaro et al. (2022).

5. The sedimentary record: results and interpretations

5.1. Depositional setting

The locations of the coring stations were selected after analysis of morpho-bathymetric and seismic reflection data (Fig. 3). All sites lay in isolated tectonically controlled basins close to a transtensional fault segmenting the continental margin in the Squillace basin (core CALA-20) (Capozzi et al., 2012) and splay faults accommodating plate convergence in the inner accretionary wedge (cores CALA-10 and -15) (Polonia et al., 2011). Core CALA-20 was collected in a confined depression on the inner plateau, at 2050 m water depth (Fig. 3). CALA-10 and CALA-15 were instead collected in two disconnected basins within the intermediate depressions of the inner CA accretionary wedge, at 2945 m and 2930 m water depth respectively (Fig. 1). The three cores (CALA-20, -10 and -15) penetrated 4.65, 3.62 and 3.42 m into the sediment (Figs. 4 and 7). Chirp profiles (Fig. 3) show that the sedimentary basins are filled by high-amplitude reflectors and homogeneous units; their seismic character suggests a coarse sandy base and a homogenite upper part (Polonia et al., 2017a). Grain size, XRF data and micropaleontological observations were performed only in

Table 3
Bathymetric information on the mentioned species includes relevant studies conducted mainly in the Mediterranean Sea (Jorissen, 1988; Sgarrella and Moncharmont Zei, 1993; van Hinsbergen et al., 2005; Frezza and Carboni, 2009) and other general knowledges (Murray, 2006; Nardelli et al., 2010).

Infralittoral taxa	Infra-circalittoral taxa	Circa-bathyal taxa	Bathyal taxa
Adelosina longirostra	*Asterigerinata mamilla*	*Amphycorina scalaris*	*Alabaminella weddellensis*
Ammonia parkinsoniana	*Bolivina aenariensis*	*Biloculinella cylindrica*	*Articulina tubulosa*
Ammonia tepida	*Bolivina dilatata*	*Biloculinella labiata*	*Astacolus crepidulus*
Cibicides lobatulus	*Bolivina striatula*	*Bolivina alata*	*Ceratobulimina arctica*
Cycloforina rugosa	*Bulimina elongata*	*Bulimina costata*	*Cibicidoides pachyderma*
Cycloforina schlumbergeri	*Buliminella elegantissima*	*Cassidulina carinata*	*Epistominella exigua*
Elphidium advenum	*Discorbis mira*	*Cassidulina laevigata*	*Ophthalmidium acutimargo*
Elphidium granosum	*Fursenkoina acuta*	*Cassidulinoides bradyi*	*Stilostomella abyssorum*
Elphidium macellum	*Hopkinsina pacifica*	*Chilostomella mediterranensis*	
Elphidium pulvereum	*Nonionella stella*	*Cibicides refulgens*	
Haynesina depressula	*Patellina corrugata*	*Dentalina communis*	
Haynesina germanica	*Quinqueloculina padana*	*Ehrembergina trigona*	
Miliammina fusca	*Quinqueloculina parvula*	*Fursenkoina tenuis*	
Miliolinella elongata	*Quinqueloculina pygmaea*	*Globobulimina pupoides*	
Miliolinella subrotunda	*Rectuvigerina phlegeri*	*Globobulimina subspinescens*	
Nonionella turgida	*Sigmoilina costata*	*Globocassidulina crassa*	
Pseudotriloculina laevigata	*Spirillina vivipara*	*Globocassidulina subglobosa*	
Quinqueloculina bosciana	*Spiroloculina angulosa*	*Glomospira charoides*	
Quinqueloculina lata	*Spiroloculina excavata*	*Gyroidina altiformis*	
Quinqueloculina milletti	*Triloculina gibba*	*Gyroidina soldanii*	
Quinqueloculina seminulum		*Gyroidina umbonata*	
Rosalina bradyi		*Hyalinea baltica*	
Rosalina floridana		*Lenticulina gibba*	
Rosalina vilardeboana		*Melonis barleeanum*	
Sigmoilina tricosta		*Pullenia bulloides*	
Sinuloculina inflata		*Pyrgo anomala*	
Vertebralina striata		*Pyrgo depressa*	
		Pyrgo elongata	
		Pyrgoella sphaera	
		Quinqueloculina stalkeri	
		Robertina translucens	
		Saidovina karreriana	
		Sigmoilina tenuis	
		Trifarina angulosa	
		Triloculina tricarinata	
		Uvigerina mediterranensis	
		Valvulineria bradyana	

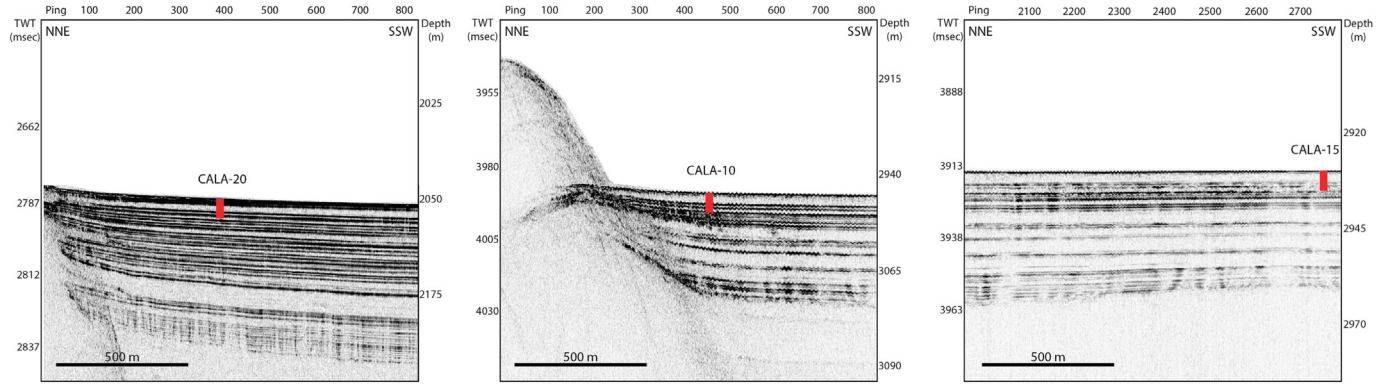

Fig. 3. Sub-bottom CHIRP profiles across the coring sites investigated in this study (see Fig. 1 for location of gravity cores). Gravity cores are represented by red rectangles on the CHIRP profiles. Seismic data have been processed and geo-referenced using the open-source software Seisprho (Gasperini and Stanghellini, 2009).

core CALA-20. We describe in detail this core and use the other two cores for lateral correlation of sedimentary units in the three different basins.

5.2. Sediment facies in core CALA-20

Core CALA-20 records sedimentation during the last ~7 ka, as suggested by the radiometric dating at the base of the core (uncalibrated 6850 ± 50 yr, calibrated 7330–6975 yr BP, Fig. 4 and Table 2). The stratigraphic reconstruction is based on the identification of peculiar marker beds through the analyses of radiometric ages, XRF data, grain size and foraminifera associations. The sediment core shows a succession of turbidite beds, hemipelagic intervals and a tephra layer.

Background marine conditions are represented by thin (1–15 cm thick) hemipelagic layers (yellow sediment units in Fig. 4) bracketing turbidite beds characterized by silty sediment with mode between 7 and 8 phi (medium to fine silt). The planktonic foraminifera in the hemipelagic sediments are typical of the recent Mediterranean Sea (Pujol and Vergnaud Grazzini, 1995), while benthic foraminifera assemblages show the nearly exclusive presence of outer shelf-bathyal and bathyal taxa, the former mainly represented by *Articulina tubulosa*, low values of specimens/g and a significant correlation with peaks of Ca/Ti (Fig. 5, Table 3). The total thickness of hemipelagic layers is only 54 cm, implying that resedimentation processes in this basin, including tephra deposition, represent 88% of total sedimentation.

The dark unit at the base of the core represents sapropelitic sediment characterized by silty mud with sand content varying between 6.6% and 13.0%. XRF data show an increase in Ba, S, Cl and a peak in Mn/Ti ontop the sapropel bed, as described in other studies (De Lange et al., 2008). Radiometric dating (Table 2) suggests that it represents the upper part of sapropel S1 (S1 in Fig. 4). Micropaleontological analyses of samples within sapropel bed S1 shows it is totally barren of benthic foraminifera.

A fine to medium sized ash layer occurs between 246 and 256 cm core depth. It is made up of micro-pumice and marked by geochemical anomalies (high Sr, Zr, Ba). This interval is totally barren of foraminifera. It was certainly deposited after 3285–2820 BP (radiometric age at 286 cm, Table 2).

Major turbidite beds in this core are marked by sharp peaks in grain size at their base (Fig. 4) while only some of them have a clear MS signature (T2, T5 and T9). They are characterized by varying geochemical composition and foraminifera association, including benthic species displaced from diverse bathymetric environments (Table 3). We identified 17 turbidite beds (T1-T17 in Fig. 4 and Table 5) with thicknesses between a few centimetres to 1.5 m (T5 in Fig. 4). They are generally normally graded, while turbidites T5, T7, T10 and T16 show multiple separate textural pulses within the lower part of the turbidite (a1, a2, a3 in Fig. 4), without hemipelagic sediment in between, each with different grain size gradation and geochemical composition. They can be described as amalgamated turbidites with distinct pulses sensu Van Daele et al. (2017) resulting from synchronous-triggered turbidity currents or as multi-pulsed and stacked turbidites sensu Nelson et al. (2012), that are typical for ST generated by a single earthquake as described in the southern Ionian Sea (Polonia et al., 2017a, 2017b).

Turbidite characterization is obtained from geochemical and micropaleontological data that together with grain size help defining the composition and structure of distinct layers within the turbidite beds and sediment source. Turbidites are usually characterized by a sharp increase in sand (up to 70% and MD = 3.5 for T10), Zr and Fe content and density and diversity of benthic foraminifera (Fig. 6). The increase in diversity in these levels is mainly due to the contribution of foraminifera from the continental shelf areas (inner and outer shelf). In these levels, the outer shelf-bathyal and bathyal species decrease in percentage, but still remain significant (Fig. 6). The most obvious marker of the turbidites are foraminifera displaced from the continental shelf, which on average take on frequencies of over 30% in these levels (Fig. 6). In almost all turbidites, inner shelf foraminifera predominate over shelf ones. In turbidites T2, T3, T5, T9, T12, T15 and T16 vegetated remains pertaining to marine phanerogams were observed.

5.3. Interbasin turbidite correlation: cores CALA-10 and CALA-15

Since the number of turbidites (roman numerals to the right of the individual logs) is different in the three basins, core correlation was based on radiometric dating (yellow rectangles in Fig. 7 and Table 2), marker beds (tephra layer and sapropel S1) and thickness/structure of turbidites. In cores CALA-10 the total number of turbidite beds is 12 while core CALA-15 sampled only 10 turbidites (Fig. 7). Core CALA-15 sampled the same stratigraphic interval as core CALA-20 but the resedimented units have different thicknesses. On the other hand, core CALA-10 sampled an older stratigraphic interval that includes the entire sapropel S1, as shown by radiometric ages at the core bottom (Table 2) in agreement with the basal part of sapropel bed S1 (De Lange et al., 2008; Polonia et al., 2015).

The tephra layer occurs in all cores with a maximum thickness in core CALA-15. It can be correlated to the tephra of core CALA-20

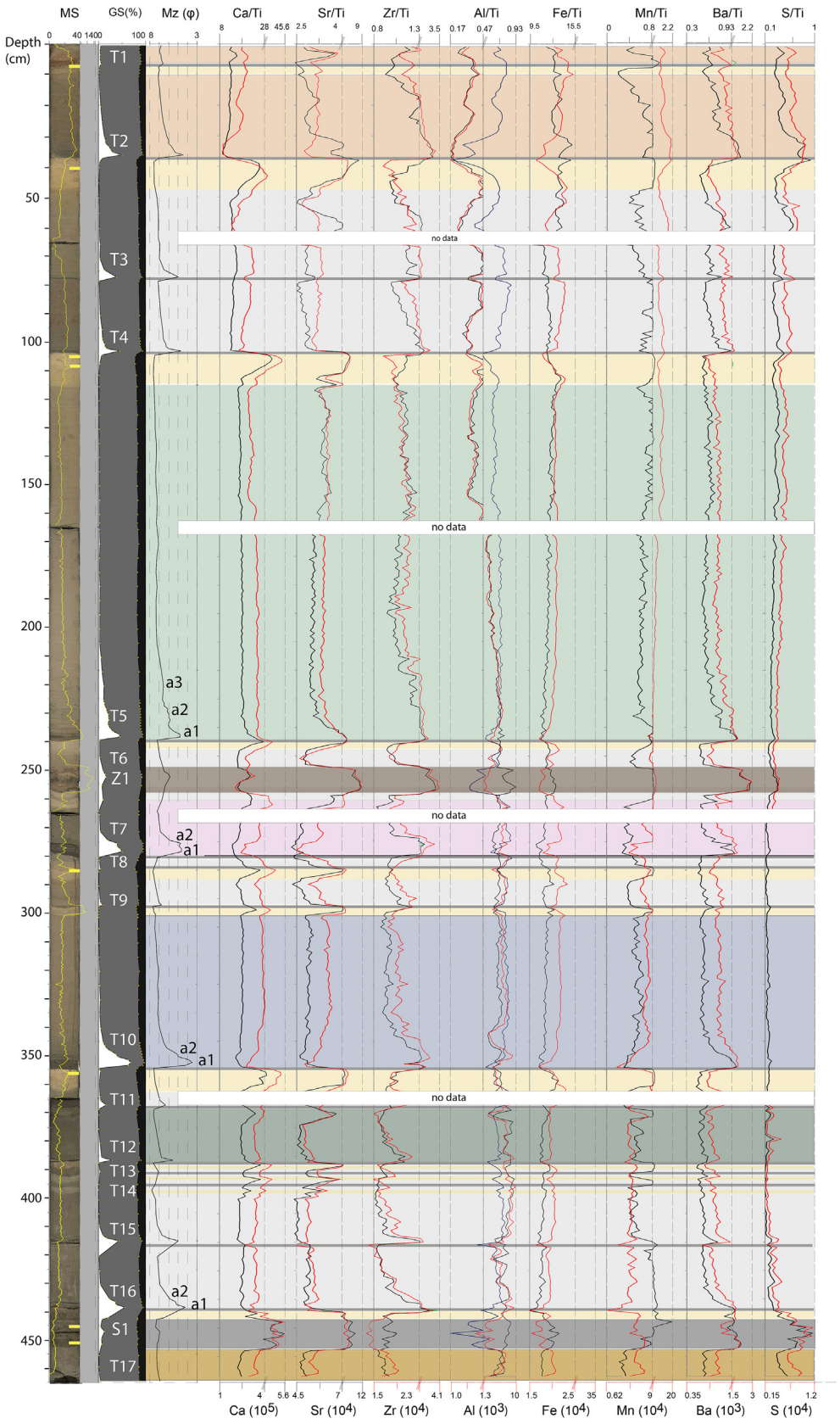

Fig. 4. Log of core CALA-20. From left to right: photograph with high-resolution magnetic susceptibility in yellow, grain size % (GS) with mean diameter (Mz) in black, subdivision in individual turbidite beds (identified by different colors) and hemipelagic units (yellow units), and XRF data plot along the study sample. Yellow rectangles on the core photograph represents ^{14}C dated samples (Table 1). a1-a3: sand pulses within the T5, T7, T10, T16 turbidites.

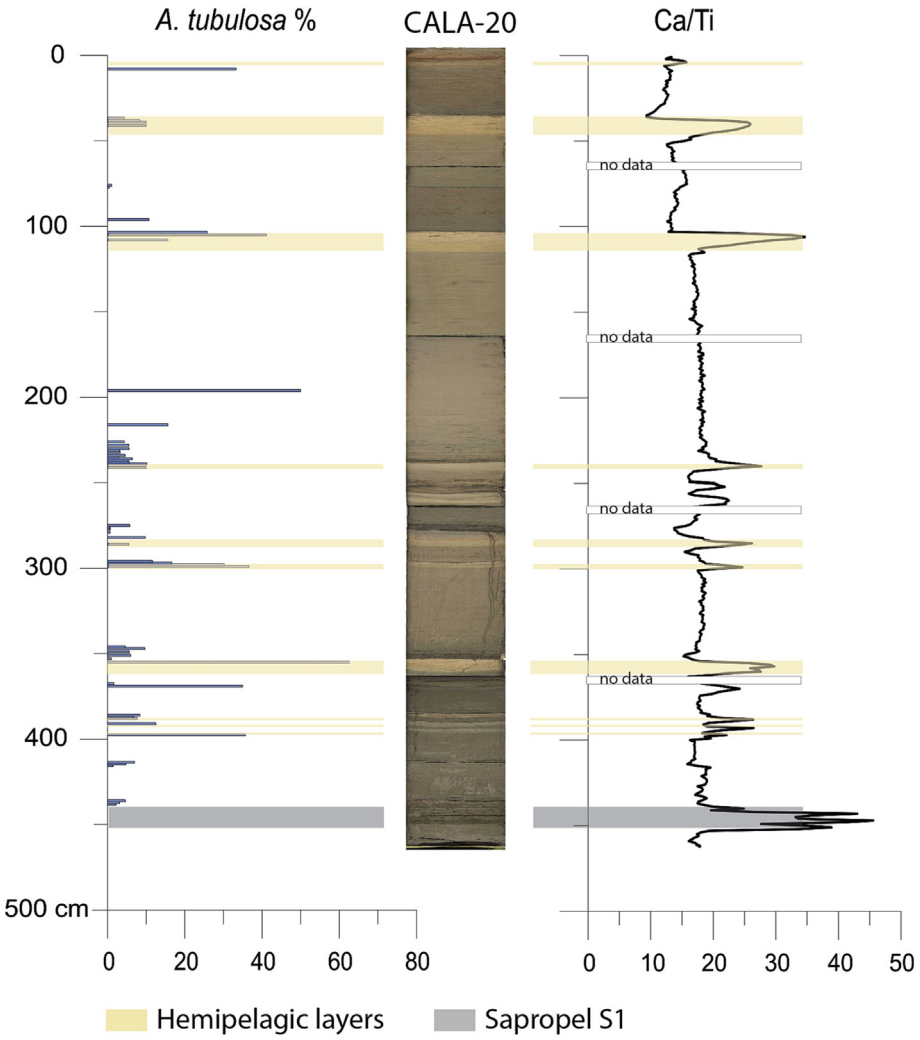

Fig. 5. Relative frequency distribution of the bathyal foraminifer *Articulina tubulosa* in the CALA20 core, in comparison with core lithology and Ca/Ti ratio distribution.

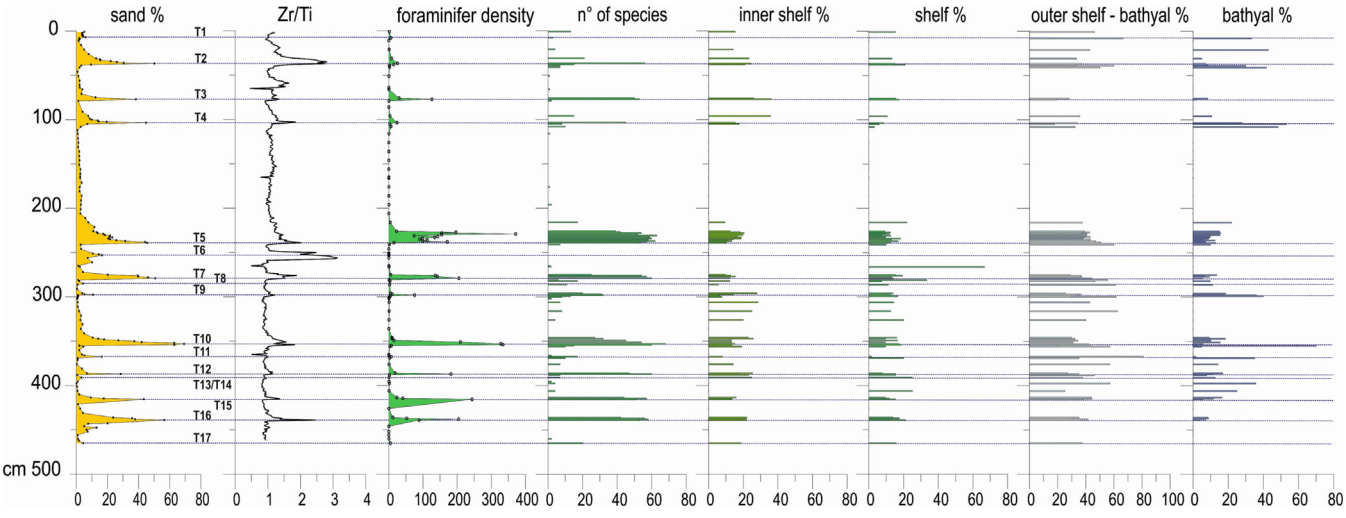

Fig. 6. Sand percentage distribution, Zr/Ti ratio in comparison with foraminifers association of the core CALA20. Foraminifer density as number of specimens/dry total weight, n° of species and distribution of the diverse foraminifer species following their deep-water preference grouped into categories as follows: inner shelf (infralittoral), shelf (infra- and circalittoral), outer shelf - bathyal (200–1000 m) and bathyal (>1000 m).

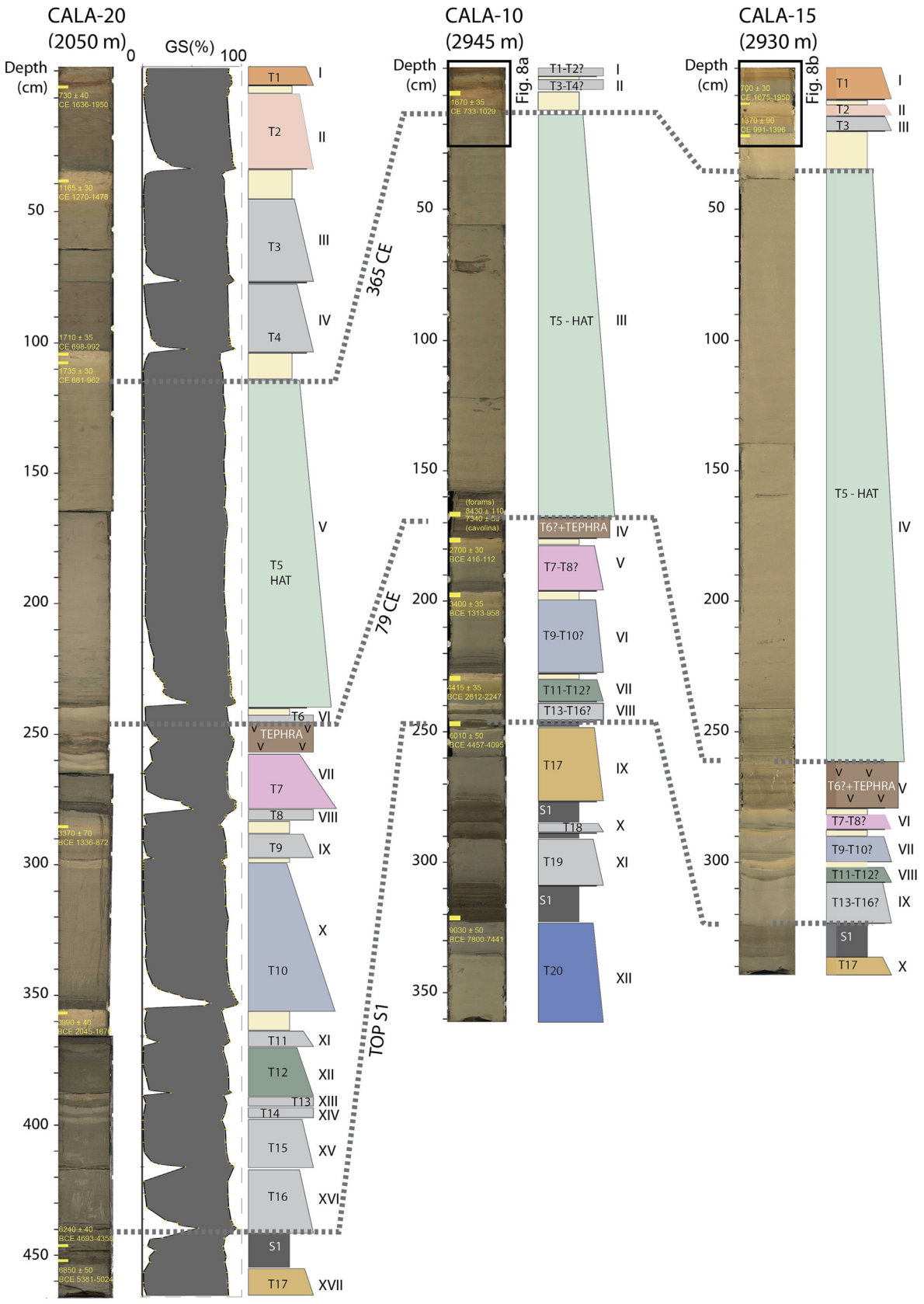

Fig. 7. Correlation of stratigraphic units in the different cores analysed in this study. From left to wright: core CALA-20, CALA-10 and CALA-15. Roman numerals to the right of the individual logs represent progressive number of the turbidite beds in the three cores. T1-T20: correlative turbidites in the three basins. Hemipelagic units are identified in yellow while major turbidite beds are represented by different colors (T1: brown; T2: light pink; T5: green; T7: dark pink; T10: blue; T12: dark green; T17: light brown; T20: dark blue). The correlation between the different turbidite beds is based on sedimentological, geochemical and micropaleontological data. The tephra layer Z-1 is indicated by the dark brown layer while sapropel S1 is indicated by the dark grey pattern.

according to stratigraphic position, radiometric ages and chemistry (see sections 5.4).

The thickest turbidite bed in core CALA-20 (T5) corresponds to turbidite III and IV in cores CALA-10 and CALA-15, respectively. This correlation is based on radiometric ages above the turbidite bed and on the observation that it lies ontop the tephra layer in all the three cores. T5 reaches its maximum thickness in core CALA-15, twice relative to core CALA-20.

The turbidites above T5 in cores CALA-10 are two thin events that cannot be clearly correlated with a specific turbidite in core CALA-20 because only one radiometric date below the base of the turbidite-II is available (Fig. 8). Considering the thickness of hemipelagic layers bracketing the turbidite beds in all cores, the most likely interpretation is that turbidite-I corresponds to T1 (or T2) and turbidite-II to T3 (or T4) but we cannot discharge other combinations of the 4 turbidites.

Core CALA-15 shows three turbidites above T5 (turbidite-I, -II and -III in Figs. 7 and 8). Radiometric ages from hemipelagic samples between the turbidite beds suggest that turbidite-I may corresponds to T1, turbidite-II to T2 and turbidite-III to T3, implying that T4 was probably not deposited in core CALA-15 or was eroded by T3.

Based on sediment structure, radiometric ages and turbidite thickness we propose a correlation with core CALA-20 also for the turbidites below T5 even though this correlation is less constrained (Fig. 7). Core CALA-10 includes 3 resedimented beds older than T17 (turbidite-X, -XI and –XII) that interrupt anoxic seafloor conditions during sapropel S1 deposition as observed in other

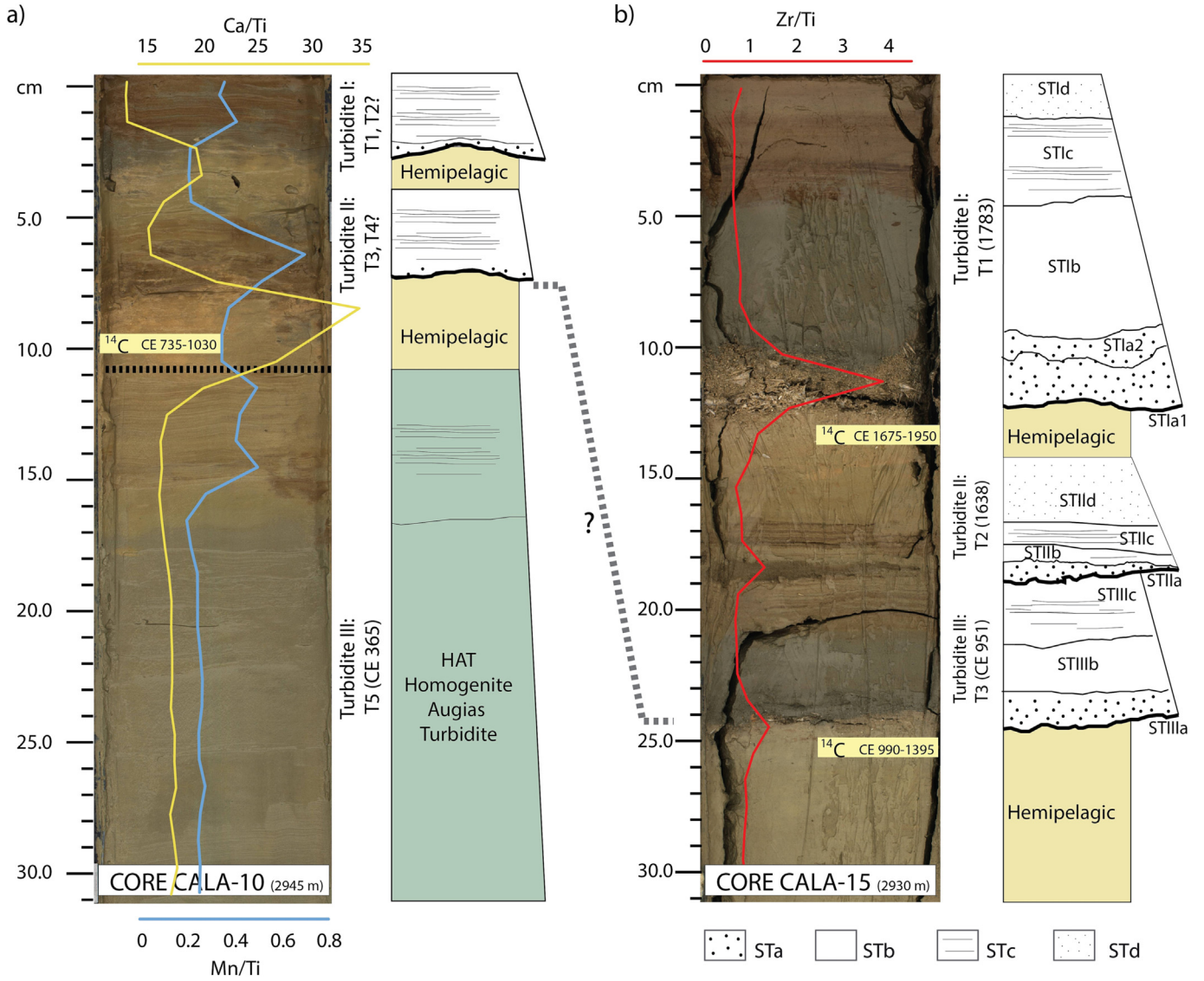

Fig. 8. (a) Enlarged photo and stratigraphic log of turbidites I, II, and III in core CALA-10 with super-imposed Ca/Ti (yellow line) and Mn/Ti (blue line) elemental concentrations. Ca/Ti marks hemipelagic intervals, while Mn/Ti is higher in correspondence of the turbidite beds. (b) Enlarged photo and stratigraphic log of turbidites I, II, and III in core CALA-15 with super-imposed Zr/Ti (red line) elemental concentration that marks the turbidite basal sandy units. In this core, turbidites II and III are not separated by hemipelagic sediment. Each turbidite shows a complex structure with cyclic ordered sediment units (STa, STb, STc, STd) marked by different colors and grain size whose origin might be related to different processes during seismo-turbidite deposition in a confined basin as described in the southern Ionian Sea for the strong earthquakes occurred in CE 1908, CE 1693 and CE 1169 (Polonia et al., 2017a, 2017b). STa: multiple sandy stacks that are deposited from synchronous multiple slope failures and turbidity currents; STb: homogenite graded mud unit deposited by the waning flows of the multiple turbidity currents that are trapped in the confined basin; STc: laminated unit that results from seiching of the confined water mass; STd: seismo-turbidite cap deposited by the slow settling suspension cloud.

cores collected in different physiographic settings of the CA (Polonia et al., 2015).

Not all the described turbidites are separated by hemipelagic intervals implying that they can be either identified as separate events or depositional pulses within the same turbidite. However, the structure of the turbidites where they are more expanded (for example turbidite-II and –III in core CALA-15, Fig. 8), reveals cyclic patterns of sediment units (STa-STd) for each resedimented bed similar to seismo-turbidites in confined basins (Polonia et al., 2017a). This observation suggests that these turbidites, even though not separated by hemipelagic sediment, represent separate events and not depositional pulses within the same turbidite.

If we assume that only thick turbidite beds in core CALA-20 represent major events that might have affected all depositional settings, including the more distal basins of cores CALA-10 and -15, we can deduce that T2, T4, T8, T9, T11, T13, T14, T15 were not deposited or eroded in core CALA-10 while core CALA-15 missed the turbidites T4, T8, T9, T11, T13, T14, T15 (non deposition or basal erosion).

5.4. Tephrostratigraphy

The tephra deposit recognized in cores CALA-20, CALA-10 and CALA1-5 occurs at 257 cm, at 175 cm and at 278 cm below seafloor, respectively. It displays a thickness from ca. 8 cm in core CALA-20 and CALA-10 up to 17 cm in core CALA-15 (Figs. 4 and 7). In core CALA-20, the basal contact of the tephra is irregular. In cores CALA-10 and CALA-15 the deposit displays sharp contacts with the underlying hemipelagite and the overlying turbidite deposits and laminated internal structures. The tephra consists of a fine ash made up of angular to sub-angular light grey and white leucite-bearing micropumice with spherical vesiculation. A minor dark component represented by lithics and microcristalline juveniles along with loose crystals of leucite and abundant biotite also occur (Supplementary Material 2). In addition, a bioclastic component was found in core CALA15. This feature, coupled with sedimentary structures observed at the same site, might be the result of multiple contemporaneous volcanoclastic resedimented beds deposited during the main volcanic event. Samples CALA-20/255 and CALA-10/174 have been selected for major-element characterisation. They have been labeled according to the core where they have been sampled and the depth below sea floor (cm) at which they occur. According to the TAS classification diagram, the analyzed glasses have a K-alkaline affinity and a phonolitic composition (Fig. 9a), which is typical of the Somma-Vesuvius products erupted during the last 3 kyr (eg. Melluso et al., 2022). Chemical features of both samples (Fig. 9 and Table 4) along with lithology (e.g. occurrence of leucite and analcime) and stratigraphic position, likely relate them to the 79 CE plinian event that produced a widespread tephra in the Central Mediterranean (Z-1, Keller et al., 1978; Insinga et al., 2020; Doronzo et al., 2022). In detail, as clearly shown in the FeO_{tot} vs CaO diagram (Fig. 9b), the composition of both white and grey pumice, which typically characterize the fall sequence on land (Lirer et al., 1973), occur at these distal sites.

5.5. Turbidite emplacement time

5.5.1. Radiometric dating

The age model constructed from dated samples provides the emplacement time of each turbidite bed with uncertainties related to the method. Table 2 summarizes radiometric ages obtained on foraminifera tests selected from 1 cm thick samples within the hemipelagic units between the turbidite beds.

The mean hemipelagic sedimentation rate as deduced through radiometric dating for cores CALA-20 and CALA-10 is 0.073–0.077 mm/yr and 0.047–0.049 mm/yr respectively (1 cm of hemipelagic sedimentation integrates about 130–137 yr in core CALA-20 and 204–212 years in core CALA-10). On the other hand, two samples spaced 6 cm apart within sapropel S1 in core CALA-20 suggest that the rate of hemipelagic sedimentation during sapropel S1 is 0.098 mm/yr implying that under sapropel S1 conditions, 1 cm thick sample used for radiometric dating, integrates an age of about 100 years. This is in good agreement with hemipelagic sedimentation rates reported in the deep Ionian Sea (Polonia et al., 2013a).

5.5.2. Ages deduced from radiometric dating and sedimentation rates

As samples were collected some cm above the top or below the base of the turbidites, the emplacement time for the turbidites has to be estimated considering the time interval corresponding to the distance between the dated sample and the resedimented deposit. We used these data to deduce the emplacement time of each turbidite bed (Tables 6 and 7).

The deposition time window of the thickest turbidite T5 (BCE 5-CE 310 in core CALA-20 and CE 100–420 in CALA-10; Tables 6 and 7) correlates with both the CE 365 Crete earthquake and tsunami and the predecessor of the 1783 event that occurred shortly before 374 CE. This latter was found in the paleoseismic trenches across the Cittanova fault and it is precisely dated by an epigraph stored in the Reggio Calabria Archaeological Museum.

Above T5, 4 other turbidite beds were emplaced during the last millennia in core CALA-20 that provides the more continuous and expanded record for these recent events. The T1 and T2 deposition time windows (CE 1675–1840 and CE 1540–1710 or CE 1530–1755, respectively) suggest a link with two seismic sequences that happened in CE 1783 (mainshocks 5–7 February and 28 March) and CE 1638 (mainshocks 27–28 March and 9 June) respectively. The T3 deposition time window is CE 720–960 in core CALA-20 and CE 735–1030 in core CALA-10, while T4 emplacement time window is 700–990 CE in core CALA-20. The ages of turbidites T3 and T4 are very similar suggesting two events very close in time. They match the age, within the uncertainties of the method, of the paleo-earthquakes recognized along the Lakes fault dated in the 7th century CE (Galli et al., 2007) and the 951 CE earthquake along the Rossano fault (Galli et al., 2010).

The tephra layer was deposited during the Pompei eruption in 79 CE and turbidite T6 was deposited immediately after.

Turbidites T7-T10 emplacement times are less constrained both in core CALA-20 and CALA-10 (Tables 6 and 7). Turbidites T7 and T8 deposited in the time windows 2685–3155 BP (CALA-20), being compatible with an ancient predecessor of the 1783 earthquake originated from the Cittanova fault around 2900 BP. The age of the same turbidite in core CALA-10 is 2045–2575 BP and that derived from the sample below its coarse base is 2905–3260 BP, 500–700 years older than the age derived from radiometric dating above the turbidite tail. This suggests that in this basin basal erosion might occur during turbidity current propagation. In turn, T9 sedimented in 3080–3560 BP (CALA-20) and 3315–3475 BP in core CALA-10 (where this age refers to T10 as well). In this core the sample below the base provides a 600–800 years older age (3985–4355 BP) suggesting again basal erosion. T10 emplacement time is 3625–3995 BP in core CALA-20. This time window correlates with the event recorded by the Cittanova fault around 3.5 ka. Turbidites from T11 to T16 are not separated by hemipelagic sediment and thus their age cannot be reconstructed by available radiometric ages. However, we can deduce that the uppermost T11-T12 turbidites were deposited around 4275–4680 BP in core CALA-20 and 4400–4770 BP in core CALA-10.

Sapropel S1 was deposited in the time window 5945–6305 BP and 9390–9750 BP in core CALA-10 while the top of sapropel S1 is dated 5625–5995 BP in core CALA-20. Within the sapropel we identified 4 turbidite beds (T17-T20). T17 that deposited around

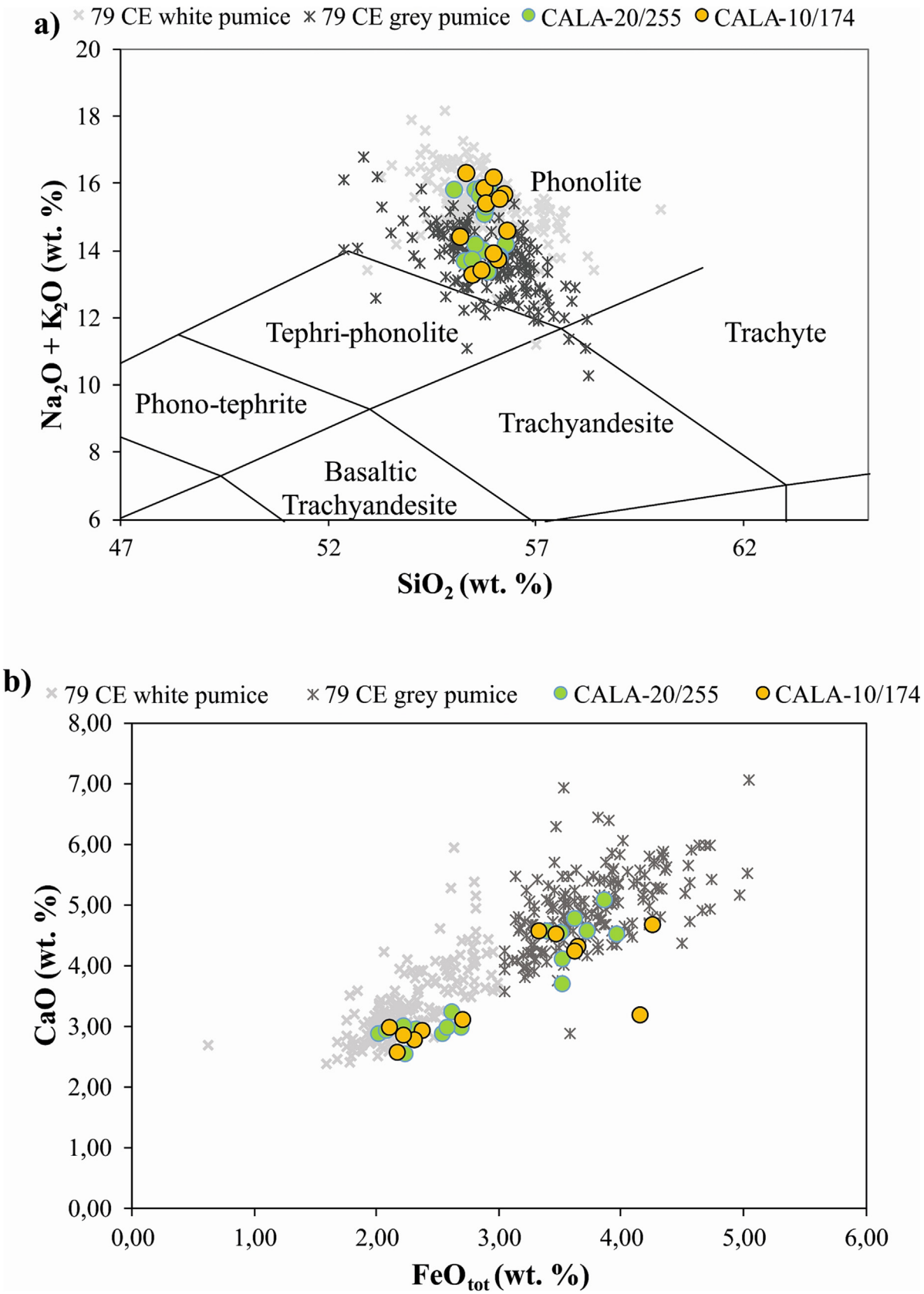

Fig. 9. (a) Total alkali/Silica (TAS; Le Maitre, 2005) classification diagram and (b) FeO_{tot} vs CaO diagram with composition of the studied tephra found in cores CALA20 and CALA10 and correlated to the CE 79 event. Single glass data from proximal deposits (white and grey fall pumice; Santacroce et al., 2008) have been reported for comparison.

Table 4
Single glass chemistry of the studied tephra. All analyses are recalculated water-free to 100%. The original totals are reported.

CALA20/255																	
SiO_2	55.44	55.39	54.42	54.97	54.99	54.52	54.19	55.16	55.00	55.00	55.12	54.75	55.04	55.20	55.29	54.64	54.97
TiO_2	0.38	0.32	0.29	0.25	0.24	0.27	0.27	0.23	0.31	0.33	0.26	0.23	0.05	0.21	0.42	0.37	0.39
Al_2O_3	20.94	21.03	22.64	22.42	20.53	21.93	20.47	22.43	22.48	21.02	22.46	22.54	22.64	22.42	20.98	20.81	20.79
FeO_{tot}	3.46	3.35	2.52	2.58	3.68	2.65	3.79	2.21	1.99	3.57	2.31	2.19	2.55	2.06	3.47	3.90	3.47
MnO	0.16	0.17	0.13	0.05	0.17	0.13	0.18	0.21	0.12	0.13	0.15	0.24	0.16	0.26	0.13	0.18	0.24
MgO	0.44	0.22	0.25	0.21	0.59	0.15	0.58	0.19	0.18	0.50	0.14	0.11	0.17	0.18	0.43	0.52	0.46
CaO	3.63	4.51	2.84	3.19	4.51	2.92	4.97	2.50	2.84	4.70	2.90	2.96	2.92	2.88	4.04	4.44	4.49
Na_2O	7.18	7.44	6.94	8.63	5.88	9.27	5.43	7.39	7.84	6.68	7.90	8.41	8.13	8.07	6.95	5.97	6.76
K_2O	6.78	6.18	8.70	6.22	7.93	6.25	7.95	8.27	7.80	6.49	7.57	6.95	6.93	7.50	6.68	7.52	7.24
P_2O_5	0.05	0.09	0.13	0.00	0.15	0.06	0.15	0.12	0.15	0.06	0.10	0.00	0.02	0.10	0.17	0.10	0.12
F	0.63	0.15	0.40	0.55	0.15	0.91	0.59	0.43	0.47	0.42	0.23	0.82	0.53	0.46	0.54	0.53	0.28
Cl	0.75	0.84	0.72	0.93	0.66	0.92	0.76	0.70	0.74	0.88	0.80	0.75	0.73	0.65	0.75	0.76	0.69
Ba	0.12	0.32	0.00	0.00	0.52	0.00	0.64	0.14	0.10	0.21	0.06	0.06	0.11	0.00	0.13	0.24	0.09
Original Total	96.71	96.95	98.44	97.40	97.63	99.66	95.94	98.10	97.86	97.82	97.14	97.35	98.22	99.20	96.90	97.40	97.18

CALA10/174												
SiO_2	54.66	55.04	55.34	54.58	54.39	55.27	55.15	55.01	55.37	55.40	55.48	55.70
TiO_2	0.19	0.16	0.43	0.26	0.42	0.47	0.21	0.47	0.15	0.17	0.20	0.56
Al_2O_3	22.20	22.35	20.86	20.91	21.00	20.92	22.11	21.30	22.15	22.52	22.52	20.52
FeO_{tot}	2.35	2.28	3.28	4.19	3.60	3.58	2.68	3.43	2.19	2.08	2.15	4.11
MnO	0.22	0.21	0.09	0.12	0.19	0.03	0.12	0.21	0.16	0.19	0.07	0.15
MgO	0.17	0.15	0.50	0.55	0.46	0.47	0.26	0.56	0.14	0.07	0.08	0.22
CaO	2.88	2.73	4.50	4.58	4.23	4.17	3.07	4.45	2.80	2.94	2.55	3.13
Na_2O	6.83	7.32	5.83	5.98	5.60	6.07	6.92	6.73	6.93	8.09	6.68	5.02
K_2O	9.26	8.31	7.68	7.09	8.60	7.66	8.27	6.49	8.49	7.22	9.33	9.40
P_2O_5	0.00	0.10	0.08	0.10	0.06	0.04	0.00	0.09	0.05	0.00	0.00	0.06
F	0.75	0.69	0.75	0.87	0.68	0.75	0.71	0.75	0.62	0.81	0.65	0.80
Cl	0.43	0.67	0.58	0.29	0.67	0.52	0.31	0.48	0.66	0.50	0.29	0.17
Ba	0.07	0.00	0.05	0.49	0.13	0.03	0.18	0.04	0.30	0.00	0.00	0.15
Original Total	96.90	97.45	97.24	96.88	95.96	94.74	98.18	98.88	95.85	98.01	97.77	96.02

6975–7330 BP (CALA-20) and 6045–6405 BP (CALA-10), might correlate with another paleo-earthquake generated by the Cittanova fault around 6.2 ka. T19 emplacement time is around 8390–8750 BP while the oldest T20, deposited probably between 9490 and 9850 BP, matches the event sourced by the Cittanova fault around 10 ka.

5.5.3. Age model

We built a deposition model for core CALA-20 (Fig. 10) and core CALA-10 (Supplementary Material 3) with the computer program OxCal 4.1 (Bronk Ramsey, 2008) including information on the order of deposition of hemipelagic units and depth. The thickness of the turbidites was subtracted from the total core (Fig. 10b) and radiometric ages were introduced in the Oxcal modelling (Fig. 10b and 10c). The software derives hemipelagic sedimentation rate from a modelled time-depth curve for the dated sediments and finds mathematically a set of possible ages for each depth point in the sedimentary sequence. Turbidite age distributions at 2σ are modelled from their stratigraphic depth of emplacement into the background sequence (Fig. 10d). The age intervals derived from the OxCal modelling are larger (Supplementary Materials 4 and 5) because errors were propagated in a more precise way and because the P_Sequence used during the age modelling considers a random distribution of sedimentation within hemipelagic units and not constant as we did in the radiometric age analysis (section 5.2.2).

The thickest turbidite T5 in core CALA-20 was emplaced in a time window (CE 84–674) in good agreement with the proposed CE 365 Crete mega-tsunami and/or with the 374 CE Calabrian event. In core CALA-10 the age of T5 is 77–247 CE.

The emplacement time windows for the most recent turbidite beds T1-T4 (T1 > CE 1510, T2 CE 1205–1431, T3-T4 CE 627–824 in core CALA-20 while T1-T2 > CE 702, T3-T4 CE 666–936 in core CALA-10) are less constrained relative to those deduced through radiometric dating and sedimentation rate. T2, in particular, does not match the proposed 1638 earthquake in core CALA-20.

The ages of major re-sedimentation events below T5 (T7, T10, T12 and T17) are within large time windows. T7 might be emplaced at the onset of the first millennium BCE, T10 during the 2nd millennium BCE, T17 during the 5th millennium BCE and T20 during the 9th millennium BCE.

6. Discussion

Facies analysis, composition, micropaleontology and marker beds (sapropel S1 and tephra Z-1) have been used to correlate turbidite beds in the different basins (Fig. 7). CALA-20 contains an expanded record of each turbidite and we used it as a reference core. Based on results on core CALA-20, within errors related to the method (see section 6.2), turbidites were correlated in the three basins based on thickness, internal structure, colour, composition, and hemipelagic sediments bracketing turbidite beds (Fig. 7). Turbidite correlation is supported by radiometric dating (Tables 6 and 7).

Some differences exist in the three cores (i.e. number of turbidites, turbidite thickness and presence or absence of hemipelagic units between the turbidites); these can be explained by the different depositional setting of the coring stations. Core CALA-20 has been collected in the basin in front of the submarine canyons from the Catanzaro Straits and Punta Stilo (Fig. 2), while core CALA-10 and -15 have been collected in more distal perched basins, about 30 km apart. All these basins are not fed directly by canyons, but whereas core CALA-20 is closer to sediment source, cores CALA-10 and -15 are from slope basins within the rough morphology of the inner accretionary wedge with isolated depressions and intervening structural highs. Core CALA-10 has the lowest sedimentation rate; for this reason it sampled the oldest turbidites.

6.1. Triggering mechanism

Different factors may affect the stability of the continental margins through long-term processes (i.e. sediment loading, gas

Table 5
Turbidite composition of core CALA-20. For each recognized turbidite (T1-T20) biogenic and geochemical components are indicated.

# Turbidite	Micro	XRF
T1	Predominance of outer shelf-bathyal foraminifera, presence of inner shelf and shelf taxa, no bathyal taxa, S > 10	Sandi unit: high in Ba and Mn; Silty unit: high in Zr, Sr, Ca
T2	Predominance of outer shelf-bathyal foraminifera, presence of inner shelf and subordinate shelf taxa, limited occurrence of bathyal taxa at the base, S > 50. Charcoal and phanerogams remains	Basal sandy part: high in Sr, Zr, Fe, Ba, S, low in Al Silty part: high in Al, lower in Sr, Zr, Ba, S
T3	Predominance of inner shelf and subordinate shelf taxa; outer shelf-bathyal foraminifera < 30% and limited occurrence of bathyal taxa, S > 50, spec/g > 100. Charcoal and phanerogams remains	Sandy part: high in Zr, Al, basal peak in Sr Silty unit: high in Fe, Mn, Ba, S, Zr, Sr
T4	Predominance of outer shelf-bathyal and bathyal taxa, presence of inner shelf and subordinate shelf taxa, S > 40. Charcoal remains	High in Zr, Ba, Al that increases upwards
T5	Predominance of outer shelf-bathyal and bathyal taxa, presence of inner shelf and shelf taxa, significant increase of inner shelf taxa toward the middle section of the T5. S > 50, ind/g high and variable. Tests are often classed in size. The topmost 90 cm interval is almost totally barren of foraminifera. Charcoal and phanerogams remains	High in Sr, Zr, Mn and Ba but only in the basal part Rather constant geochemical trends within the turbidite
T6	No data	High in Al (silty turbidite)
Z-1	Totally barren of foraminifera	Ca: low in the basal part, high in the upper part High in Sr, Zr, Al, Mn, Ba
T7	Predominance of outer shelf-bathyal and bathyal taxa, presence of inner shelf and shelf taxa. Significant increase of shelf taxa towards the top of the interval. S > 50, spec/g > 200. Tests are often classed in size. Charcoal remains	Basal sandy part: high in Zr, Ba Silty part: increase in Ca, Sr
T8	Predominance of outer shelf-bathyal taxa, presence of inner shelf and shelf taxa. Significant increase of shelf taxa towards the top of the interval	High in Al (silty turbidite)
T9	At the base, predominance of outer shelf-bathyal and bathyal taxa; increasing presence of inner shelf and shelf taxa to the top, S > 20. Phanerogams remains	Two peaks of Zr in the basal part
T10	Predominance of outer shelf-bathyal and bathyal taxa at the T10 base, increase of inner shelf taxa toward the top. S > 60 and ind/g > 200 at the base and decreasing thereafter. Charcoal remains	Two peaks in Zr and high in Ba in the sandy unit
T11	Predominance of outer shelf-bathyal taxa, very limited occurrence of inner shelf and shelf taxa	No data
T12	Predominance of outer shelf-bathyal and bathyal taxa, presence of inner shelf and subordinate shelf taxa, S > 40. Phanerogams remains	High in ZR in the basal part. Fluctuations in Mn within the turbidite
T13	Comparable presence of outer shelf-bathyal, inner shelf and shelf taxa at the base, increasing occurrence of outer shelf-bathyal thereafter, S > 5, spec/g < 10	Fine, Ca-rich turbidite or hemipelagic?
T14	Outer shelf-bathyal taxa occurrence, only	Fine, Ca-rich turbidite or hemipelagic
T15	Predominance of outer shelf-bathyal taxa, presence of inner shelf and shelf taxa. S > 50, ind/g > 200 at the base and decreasing thereafter. Tests are often classed in size. Charcoal and phanerogams remains	Basal sandy part: high in Zr, Ba, Mn Silty part: increase in Ca, S
T16	Predominance of outer shelf-bathyal taxa, presence of inner shelf and subordinate shelf taxa, bathyal taxa < 10%. Tests are often classed in size. Charcoal and phanerogams remains	Basal sandy part: high in Zr, Ba Silty part: increase in Al
S1	Planktonic foraminifera and pteropods, pyrite remains	High in Ca, Srt, Ba, Mn
T17	Predominance of outer shelf-bathyal taxa, presence of inner shelf and shelf taxa, no bathyal taxa, S = 20 at the base	Recovered only the upper part of the turbidite

hydrate destabilization, tectonic deformation), while instantaneous triggers are generally represented by earthquakes, tsunamis, storms and hyperpycnal (over-density) flows. All these factors and their combination may produce turbidity currents with very similar final sedimentary deposits. For this reason, the turbidite triggering mechanisms are derived through indirect and complementary observations and uncertainties may be large.

Offshore Calabria possible processes that can trigger turbidity currents other than ground shaking are meteorological events, such as the hurricanes that affected the Mediterranean region during the last decades (Miglietta et al., 2013). Uplifting coastal mountains, combined with canyons having their head close to the shoreline, make the Ionian Sea prone to river floods and hyperpycnal flows (Casalbore et al., 2011) during metereological events. However, our post-storm abyssal cores do not show any turbidite bed that could be related to these events either in this area or in the abyssal plain offshore eastern Sicily (Polonia et al., 2017a). Moreover, flash floods that generated debris flows in the shelf and upper slope domains (Casalbore et al., 2011) did not trigger turbidity currents that travel down to deep slope basins or abyssal plain (Polonia et al., 2017a). The same results were described in other tectonically active margins such as New Zealand, where only 3% of the turbidites deposited during the last 18.000 years are related to storms (Pouderoux et al., 2012), or Cascadia, where storms apparently fail to ignite turbidity currents below 450 m water depth (Puig et al., 2004; Goldfinger et al., 2012).

A number of observations favor a seismic trigger of the Calabria turbidites. Turbidite frequency does not agree with the frequency of catastrophic floods and storms. Cyclones and storms have a quasi-seasonal recurrence time, whereas abyssal turbidites repeat every several hundred years, as earthquakes do. Moreover, the average time interval between successive turbidite beds, agrees with the time interval between major earthquakes. Major turbidites show the typical structure of seismo-turbidites in confined basins with STa-STd sediment units (Fig. 8b) that can be associated to the different sedimentary processes of a seismo-turbidite (i.e.

Table 6
AMS radiometric data for core CALA-20 and ages of single turbidite beds. 1: core ID; 2: core depth; 3: position of the dated sample relative to the turbidite; 4: uncalibrated ages; 5: calibrated ages; 6: emplacement time for the turbidites estimated considering the time interval corresponding to the distance between the dated sample and the resedimented deposit and hemipelagic sedimentation rate (see section 5.5.2); 7: likely triggering historical and paleo-earthquakes; 8: likely causative faults.T1-T17 identified turbidite beds. When turbidites might represent more than one event they are indicated as Tn-Tm.

1 Core (water depth)	2 Sample ID and core depth (cm)	3 Position relative to the turbidite	4 14C measured age BP	5 Calibrated Age (2 σ) with ΔR=0	6 Age of turbidites: dates interpolated on the top of the turbidite	7 Earthquakes	8 Faults
CALA-20 (2050 m)	V 12-13 (8)	Just below T1	730 ± 40	CE 1675-1840 (1 σ)	**T1**: CE 1675- 1840 *(if no erosion)*	CE 1783	Cittanova
		1 cm above T2			**T2**: CE 1540-1710	CE 1638	Lakes
	V 45-46 (41)	2 cm below T2	1165 ± 30	CE 1270- 1480	**T2**: CE 1530-1755 *(if no erosion)*		
		4 cm above T3			**T3**: CE 720-960	CE 951	Rossano
	IV 39-40 (105)	Just below T4	1710 ± 35	CE 700- 990	**T4**: CE 700-990 *(if no erosion)*	7th c.	Lakes
	IV 42-43 (108)	5 cm above T5	1735 ± 30	CE 680- 960	**T5**: BCE 5 - CE 310	CE 365, <CE374?	Hellenic Arc or Cittanova?
	II 20-21 (286)	1 cm below T7-T8	3370 ± 70	BCE 1335-870 [2820-3285 BP]	**T7-T8**: BCE 1205-735 2685-3155 BP *(if no erosion)*	~2900 BP	Lakes or **submarine**?
		2 cm above T9			**T9**: BCE 1610-1130 3080-3560 BP	~3500 BP	Cittanova or **submarine**?
	II 90-91 (356)	Just below T10	3990 ± 40	BCE 2045-1676 [3626-3995 BP]	**T10**: BCE 1675-2045 3625-3995 BP *(if no erosion)*		**Submarine**?
		5 cm above T11			**T11- T12**: BCE 2730-2325 4275-4680 BP	???	**Submarine**?
	I 80-81 (446)	within sapropel S1 5 cm below top S1	6240 ± 40	BCE 4693-4358 [6308-6643 BP]	**Top Sapropel**: BCE 4045-3673 5625-5995 BP	//////	//////
	I 86-87 (452)	within sapropel S1 just above T17	6850 ± 50	BCE 5381-5024 [6975-7330 BP]	**T17**: BCE 5380-5025 6975-7330 BP	~6200 BP?	Cittanova or **submarine**?

stacked sand layers, homogenites, laminites and tsunamites) as a response to the complex succession of sedimentary processes following seismic shaking and eventually tsunami propagation in confined basins (Polonia et al., 2017a).

Inter-basin correlation and spatial extent of Calabria turbidites (when they can be correlated) exceeds that reasonably expected from meteorological or river-sourced turbidite events that generally produce more local effects. Moreover, the ages of recent turbidite events that are better constrained correlate with major historical earthquakes in the area (T1-T4 in core CALA-20). Some of the pre-historical major turbidite events correlate with trench studies onshore, supporting a triggering mechanism capable of producing effects both in the marine and onshore environment. However, uncertainties in turbidite correlation exist in this area and before proposing a one-to-one correlation between turbidites and earthquakes the uncertainties need to be clearly outlined.

Table 7
AMS radiometric data for core CALA-10 and ages of single turbidite beds. 1: core ID; 2: core depth; 3: position of the dated sample relative to the turbidite; 4: uncalibrated ages; 5: calibrated ages; 6: emplacement time for the turbidites estimated considering the time interval corresponding to the distance between the dated sample and the resedimented deposit and hemipelagic sedimentation rate (see section 5.5.2); 7: likely triggering historical and paleo-earthquakes; 8: likely causative faults. T1-T20 identified turbidite beds. When turbidites might represent more than one event they are indicated as Tn-Tm.

1 Core (water depth)	2 Sample ID and core depth (cm)	3 Position relative to the turbidite	4 14C measured age BP	5 Calibrated Age (2 σ) with ΔR=0	6 Age of turbidites: dates interpolated on the top of the turbidite	7 EVENT	8 Faults
CALA-10 (2945 m)	IV 9.5-10.5 (10)	Just below T3-T4	1670 ± 35	CE 735- 1030 [920-1215 BP]	**T3-T4**: CE 735-1030 *(if no erosion)*	7th century	Lakes
		3 cm above T5			**T5**: CE 100–420	CE 365, <CE374?	Hellenic Arc or Cittanova?
	II 8-9 (168)	within T5 sandy base	8430 ± 110	Resedimented			
	II 8-9 (168)	within T5 sandy base	7340 ± 50	Resedimented			
	II 18.3-19.3 (178.3)	Just below tephra	2700 ± 30	BCE 415 - CE 110 [2060-2365 BP]	**T6, Z-1**: BCE 415 - CE 110	Pompei CE 79	
		1 cm above T7-T8			**T7-T8**: BCE 625-95 2045-2575 BP	~2900 BP	Lakes or **submarine**?
	II 38-39.5 (198)	Just below T7-T8	3400 ± 35	BCE 1315-960 [2910-3265 BP]	**T7-T8**: BCE 1315-960 2905-3260 BP *(if no erosion)*		
		1 cm above T9-T10			**T9-T10**: BCE 1525-1165 3315-3475 BP	~3500 BP	Cittanova or **submarine**?
	II 70-71 (230)	1 cm below T9-T10	4415 ± 35	BCE 2610-2245 [4195-4560 BP]	**T9-T10**: 2035-2405 BCE 3985-4355 BP *(if no erosion)*		
		1 cm above T11-T12			**T11-T12**: 2820-2450 BCE 4400-4770 BP	???	**Submarine**?
	II 87-88 (248)	1 cm below top sapropel S1	6010 ± 50	BCE 4455-4095 [6045-6405 BP]	**S1 top**: 5945-6305 BP		
		Just above T17			**T17**: BCE 4455-4095 6045-6405 BP	~6200 BP	Cittanova or **submarine**?
	I 60-61 (321)	Base of sapropel S1	9030 ± 50	BCE 7800-7440 [9390-9750 BP]	**S1 base**: 9390-9750 BP		
		10 cm below T19			**T19**: BCE 6800-6440 8390-8750 BP *(if no erosion)*	????	**Submarine**?
		1 cm above T20			**T20**: BCE 7900-7540 9490-9850 BP	~10000 BP	Cittanova or **submarine**?

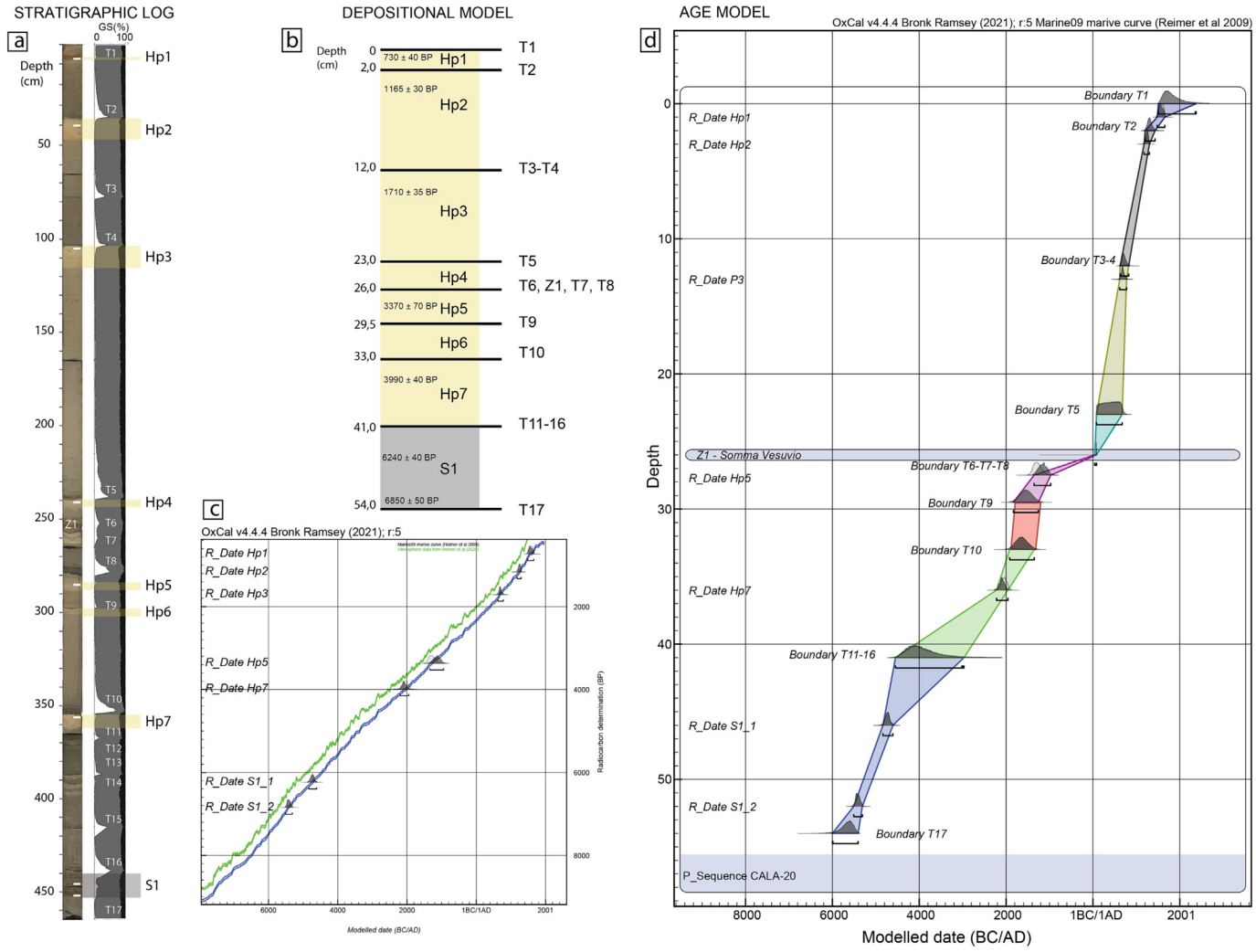

Fig. 10. Age modelling results of core CALA-20: (a) stratigraphic log, photograph and grain size presented as % in sand, silt, clay. Hemipelagic units (Hp) are highlighted by yellow rectangles and dated samples by white rectangles; (b) deposition model built subtracting the thickness of the turbidites (instantaneous sedimentary events) from the total core with uncalibrated radiometric ages of dates samples within each dated hemipelagic interval; (c) calibrated radiometric dates (2 σ) of the hemipelagic units; (d) age model built using the P_Sequence (a Bayesian model of deposition) implemented in the computer program OxCal 4.1 that assimilates sedimentation as a random process following a Poisson law (Bronk Ramsey, 2008). The model calculates the age of each corrected depth corresponding to a turbidite or turbidites (if they are not separated by hemipelagic sediment) and generates the 95.4% probability age ranges (2σ).

6.2. Uncertainties of our approach

Reconstructing the age of the resedimented beds is not trivial, especially in areas where average magnitude earthquakes occur frequently and sedimentation rate is not very high inhibiting hemipelagic sedimentation between all turbidite beds. Major uncertainties are related to: (i) analytical errors of radiometric dating; (ii) material used for dating or to coring/sampling operations that may introduce loss of material ontop the core and/or sediment contamination; (iii) identification and correlation of turbidites is often based on a geological interpretation subject to personal decisions. We summarize here the main source of uncertainties and errors and how these might affect our conclusions.

Carbon-14 dating is rather accurate and often have a margin of error lower than 5%. In our study, analytical errors in radiometric dating vary between 0.8% and 6.6% (Table 3). We did not apply a marine reservoir correction because of the lack of local data and the great dispersion of ΔR values in the surrounding regions. However, a previous work in the southern Ionian Sea took into consideration a correction calculated as the weighted mean including 2 ΔR values from published reservoir ages and the difference between the results obtained with the marine reservoir correction are 100–200 years younger than those without taking into account the reservoir effect (Polonia et al., 2013a,b). For this reason, we cannot rule out that the emplacement time windows for the Calabria turbidites might have been younger if we could have considered a marine reservoir correction.

Regarding the selected material for radiometric dating, we stress that bioturbation, although weak, might be present in the hemipelagic units, introducing a further error not included in the previous analysis. Another limitation is that each 1-cm thick sample integrates about 100–200 years of sedimentation and this implies that it is not possible to identify events too close in time or belonging to the same seismic sequence. Moreover, separate earthquakes in the same seismic sequence might produce distinct seismo-turbidites, stacked one above the other (if they occur months-years apart) or they might trigger sand pulses within the same turbidite bed (if they occur minutes/hours apart). These different contributions cannot always be distinguished. We have attempted to discriminate the different effects of seismic events belonging to the same seismic sequence in an alpine lake struck by 2 major seismic events during the 1976 Friuli seismic sequence

(Polonia et al., 2021a, 2021b) but the lacustrine environment is more conservative than the abyssal basins offshore Calabria. On the other hand, we stress that paleoseismological reconstructions based on trenches onshore might be affected by even higher uncertainties.

Together with ages derived through radiometric dating and sedimentation rate estimates, we derived also emplacement time windows through Oxcal age modelling. The regularity of sedimentation (k), with the higher values of k introduced in the model the smaller variations in sedimentation rate taken into account, is one of the inputs parameters that might influence age modeling results. We chose k = 3.0 because we assume that hemipelagic sedimentation in such a deep basin does not vary much during the Holocene, as in previous studies in the Ionian Sea (Polonia et al., 2013a, 2013b). However, we tested two different k values (k = 1 and k = 3) for core CALA-20 (Supplementary Material 6). A more variable sedimentation rate increases the width of the emplacement time window for each turbidite bed without changing much the results because major earthquakes that were proposed as likely triggering events fall within the larger time windows.

If two turbidites are not separated by hemipelagic sediment, then their age in the model output will be the same (T3-T4, T7-T8, T11-T16 in core CALA-20, T1-T2, T3-T4, T7-T8, T9-T10, T11-T15 in core CALA-10, Fig. 7 and Supplementary Materials 4 and 5), while for those turbidites that cannot be correlated in the different basins (for example T7-T8, T9-T10, T11-T12) we can only speculate that the more recent event eroded the previous one or that one of them was not deposited. If it is related to basal erosion, the turbidites might have been deposited in a synchronous way in all basins and then eroded by the more recent event. If the number of turbidites is different because some of them did not deposit in some basins, the triggering mechanism might be more local with weaker sedimentary effects. In core CALA-20 the age of T2 was derived considering radiometric ages and sedimentation rate below the base and above the top of the turbidite. The resulting emplacement time windows are very similar implying that no basal erosion occurred during the deposition of T2. For core CALA-10, on the other hand, the emplacement time windows for T7-T8 and T9-T10 derived from samples below the base and samples above the turbidite tail are different (some hundred years). For these turbidites, basal erosion cannot be considered negligible and only dated samples above the turbidites provide reliable emplacement ages.

For all the reasons above, a one-to-one correlation between seismo-turbidites and earthquakes offshore Calabria is not always possible. On the other hand, where it is possible, correlation of turbidites in widely separated sites isolated from each other imply a common source. Physiographic, oceanographic, or hydrodynamic controls fail to explain this regional occurrence and at least major turbidites may be considered as recorders of earthquake ruptures that may account for the regional consistency as demonstrated in other active continental margins (Goldfinger et al., 2012; Patton et al., 2015). Turbidites that may be correlated in the three different basins might correspond to major earthquakes, while non correlative turbidites might be related to more local events and/or to the upper plate normal faults that produce more moderate effects in the submarine environment. Oceanographic and metereological events can produce sedimentary effect in the Ionian Sea but their effects (i.e. flash flood deposits) were not reported in environments deeper than 500 m (Casalbore et al., 2011).

6.3. Correlation between turbidites and earthquakes

It is not common to have the opportunity to tie (within errors) known historical earthquakes to specific deposits: the Ionian Sea may be considered in this context as a reference region for this approach (Polonia et al., 2013a, 2017a). We have attempted a first order correlation between turbidites and major seismic events in the study region based on the analyses of earthquake catalogues and trench studies onshore even though the uncertainties are large. We propose that the uppermost four seismo-turbidites (T1-T4) can be correlated with Calabrian events that occurred in CE 1783, 1638, 951 and 7th century (Tables 6 and 7).

The emplacement age of T5 correlates well with the far field Crete event even though a local event is reported in Calabria < 374 CE (Galli and Bosi, 2002); this needs to be taken into account as a likely source for T5 emplacement. Since the < 374 CE event is considered the predecessor of the CE 1783 earthquake, we can assume that the two earthquakes are similar in magnitude and indirect sedimentary effects, if turbidite thickness may be related to the magnitude of the earthquake as demonstrated in Chilean lakes (Moernaut et al., 2014). However, the thickness of T5 is an order of magnitude larger relative to T1 and all other turbidites, suggesting that T5 is related to an exceptional event. The CE 365 catastrophic Crete earthquake produced a tsunami with basin-wide effects, from Egypt (Salama et al., 2018), to Sicily (Smedile et al., 2011), Malta (Mottershead et al., 2018) and Tunisia (Bahrouni et al., 2022). For this reason, we propose that T5 is related to the CE 365 megatsunami originated in the Hellenic Arc. This tsunami produced multiple far-field slope failures that resulted in stacked basal turbidites within isolated basins of the deep ocean. The composition of sediment in isolated basins suggests their deposition by large-scale sheet like flows similar to that caused by the Tohoku earthquake associated tsunami (Polonia et al., 2022). This high-energy event was probably capable of eroding a large amount of sediment from the continental margins including the seismo-turbidite deposited during the < 374 CE earthquake.

Between tephra layer Z-1 (CE 79) and the top of sapropel S1 (5945–6145 BP) up to ten turbidites (T7-T16) were deposited offshore Calabria. Considering core correlation in the different basins, three of these turbidites appear to be major sedimentary events (T7, T10 and T12, or the pink, blue and green layers in Fig. 7). T7-T8 emplacement time correlates with an earthquake that occurred ~2.9 ka BP on the Lakes fault (Tables 6 and 7), T9 correlates with an earthquake that occurred ~3.5 ka BP on the Cittanova fault while for T10, T11-T12 no correlation with known earthquakes onshore is possible.

During sapropel S1 deposition another 4 events (core CALA-10, T17-T20) interrupt the anoxic condition of the sea bottom, transporting shallow-water sediment to the deep basins. Radiometric ages suggest that T17 might be correlated with an earthquake that occurred on the Cittanova fault at ~6.2 ka BP while turbidites T20 fits well with the age of an earthquake that occurred at ~10 ka BP on the same Cittanova fault. For turbidite T18 and T19 no correlation with known earthquakes is possible. In core CALA-21 (Fig. 1), which was collected in the study region on top of a structural high, 9 turbidites interrupt anoxic conditions during the deposition of sapropel S1 (Polonia et al., 2015). Among these turbidites, two of them correlate well with the two 6.2 ka BP (T17) and 10 ka BP (T20) events found in this study, suggesting that the Cittanova fault might be capable of producing sediment remobilization in a wide submarine region. The structural high of core CALA-21 appears to be a more conservative depositional setting isolated from the basin floor and thus preventing thin turbidite beds from erosion during resedimentation processes. The ages of all turbidites found in core CALA-21 are included in the chronogram of Fig. 11. However, since core CALA-21 was collected more to the East, we cannot exclude that some of the turbidites were triggered by different faults within the Hellenic/Albania system.

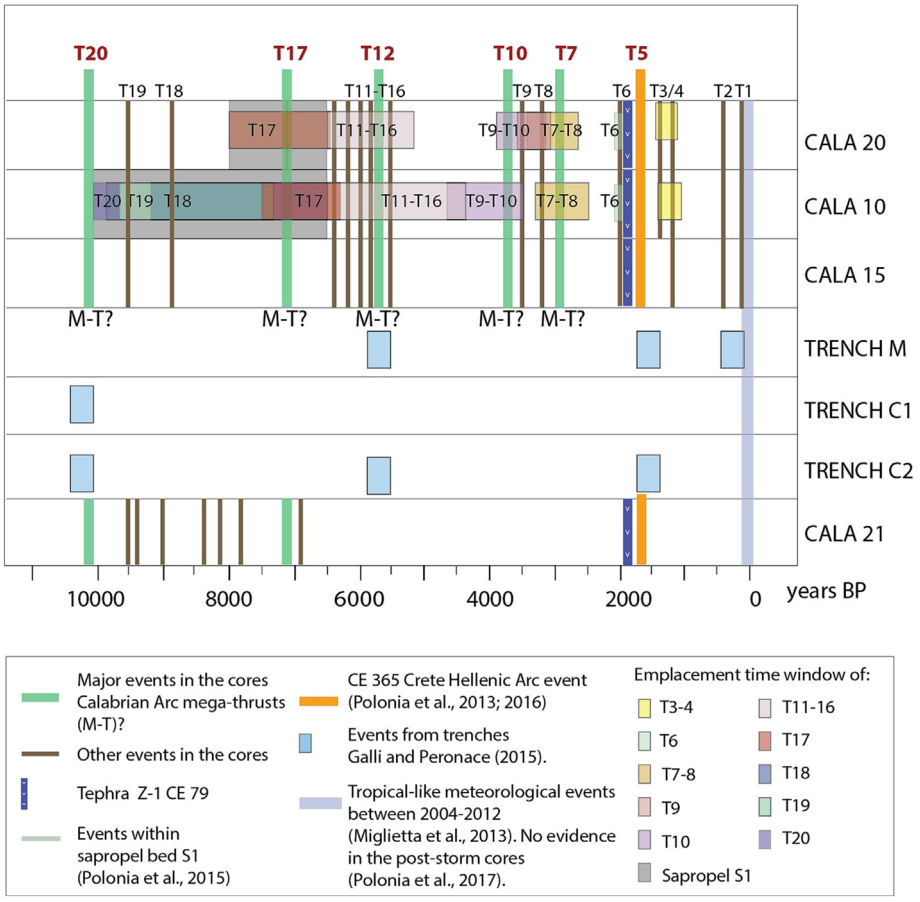

Fig. 11. Chronogram of the events identified in the gravity cores and in trenches onshore.

6.4. Sediment provenance and causative faults

Previous work on resedimentation processes in the CA has shown that during historic times, episodic deposits on the Ionian Sea basin floor are generated by earthquakes and tsunamis (Polonia et al., 2021a, 2022 and references therein). However, major issues deserving further analysis include: (1) the complexity of the sedimentary record and of the seismic sources; (2) the sensitivity of the core location in linking individual deposits to a specific earthquake; and (3) the earthquake magnitude threshold in triggering mass flows. The cores analyzed in this study provide information on these complex relationships and generally on source to sink processes.

Earthquakes may trigger sediment remobilization hundreds of kilometres from the epicentre but the sediment source and slope failures are generally close to the epicentral area (tens to hundreds km, Patton et al., 2015) depending on magnitude of the earthquake, distance to the hypocentre and ultimately seismic loading (Douglas, 2003). However, the failure threshold depends on several other parameters such as the material properties, local pore pressure, presence of weak layers, slope angle and earthquake history.

Previous studies suggest that earthquake magnitude thresholds are required to generate seismo-turbidites; however, thresholds vary in different basin settings depending on rupture depth and earthquake type (Nakajima and Kanai, 2000; Strasser et al., 2013; Van Daele et al., 2013, 2014). The Ionian Sea confined basin setting seems to have lower thresholds (Mw 6.2) for turbidite generation (Polonia et al., 2017a) than in unconfined basins like Cascadia and Japan (Mw 7.2) (Nakajima and Kanai, 2000; Goldfinger et al., 2012; Strasser et al., 2013). This might be related to the complex interplay between uplifting coastal mountains, high sediment discharge on the narrow continental shelves and steep slopes of the continental margin offshore Calabria (Fig. 2). The wide and complex canyon systems together with the seabed morphologies of the Ionian continental shelf indicate that intense erosion and mass wasting processes produce an unstable continental margin (Ceramicola et al., 2021). A wide range of slope instability phenomena include isolated landslide scars along slopes and headwall and sidewall niches in submarine canyons and indicate retrogressive activity of the canyon heads and instability of the shelf margin (Cuppari et al., 2004).

The 20 turbidite events deposited during the last 10 ka represent a minimum value because we cannot exclude a larger number of seismo-turbidites during the Holocene, i.e. we are analyzing only the major ones that might have eroded other minor events. In the abyssal domain, erosion is usually negligible (Gutierrez-Pastor et al., 2009) as suggested by the thickness of hemipelagic intervals between turbidite beds that correspond nicely to the interval between intervening earthquakes (Polonia et al., 2013a) but in the study region it cannot be ruled out, especially in cores CALA-10 and -15. Within this uncertainty, the average recurrence time of re-sedimented deposits in this area is about 500 years; however, it is not constant in time, showing periods of enhanced activity separated by more quiescent intervals (Fig. 11). The same trend was found in core CALA-21 (Fig. 1) where the average recurrence of seismo turbidites is about 500 years but it varies between 100 and 700 years (Polonia et al., 2015).

It is generally recognized that 0.1% g – 0.2% g PGA is the threshold of stability for the triggering of landslides in marine sediments (Keefer, 1984; Meunier et al., 2007) but PGA threshold may reach

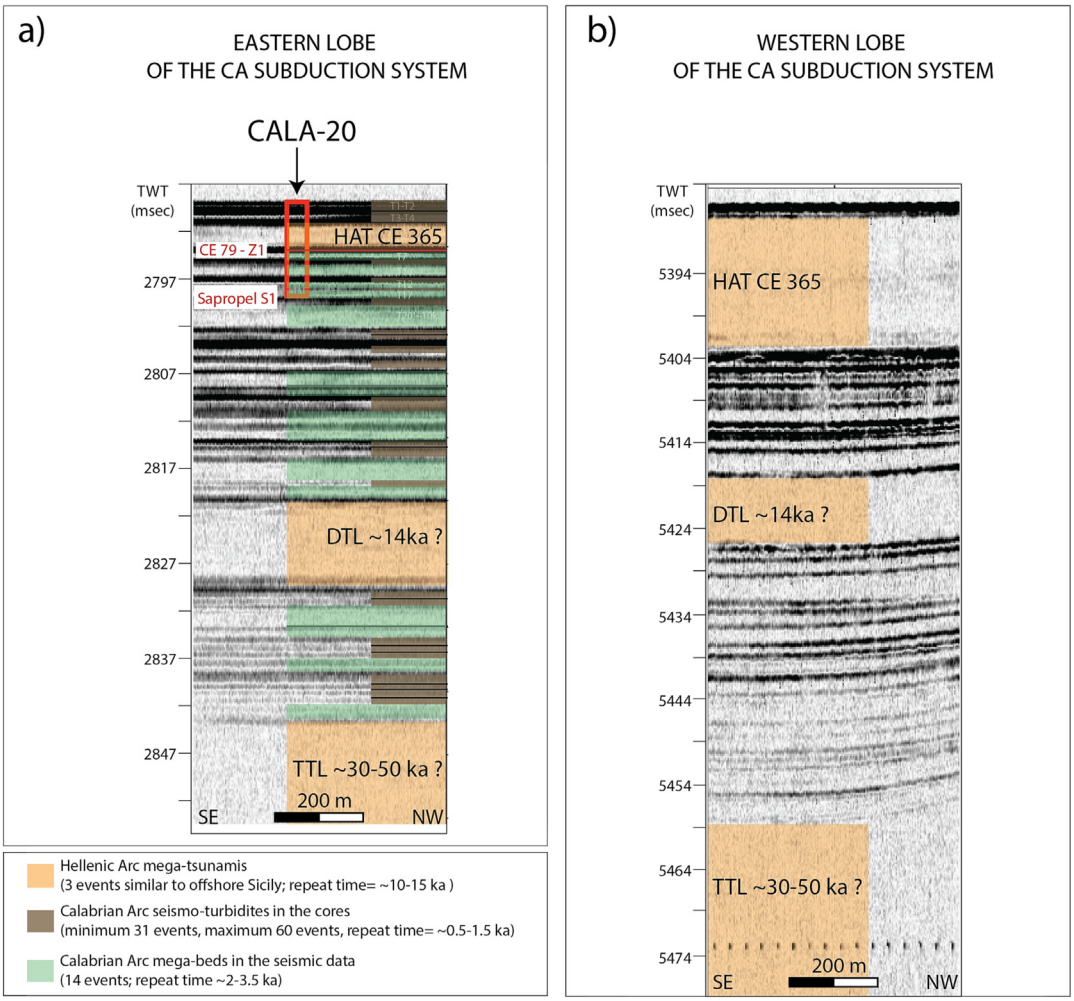

Fig. 12. CHIRP sub-bottom profiles in two different basins of the Calabrian Arc. (a) Chirp profile acquired during CALA-20 core collection (see location in Fig. 1). (b) Chirp profile collected in the abyssal plain belonging to the western lobe of the subduction system where the slab is already detached (Polonia et al., 2017b). Three similar megaturbidites in both CHIRP profiles reveal basin-wide events possibly triggered by the Hellenic Arc far field sources. The HAT (Homogenite-Augias Turbidite), the DTL (Deep Transparent Layer) and TTL (Thick Transparent Layer) megaturbidites are highlighted in the profiles by orange colors (see also Polonia et al., 2022). The low reflectivity seismic facies of these megabeds in the Chirp profile is related to the upper rather homogeneous part of the megabed. The DTL elemental composition suggests a similar source region as the HAT megaturbidite and an age of about 14 ka (Polonia et al., 2013b). The age of the oldest megabed is still unknown. Seismic data have been processed and geo-referenced using the open-source software Seisprho (Gasperini and Stanghellini, 2009).

up to 0.6% g (Strasser et al., 2007; Dan et al., 2009). Considering the unstable Calabria continental margin we can assume that the lower limit is more representative for the study region where a lower threshold for earthquake triggering may be related to the peculiar physiography of this basin and to the presence of tephra layers such as Z-1 that may act as weak horizons enhancing slope instability (Harders et al., 2010; Sammartini et al., 2019 and references therein).

Since the onshore earthquakes are located close to the coastline, we have considered the attenuation laws between their epicentre and the coastline implying that this distance is entirely onshore. If we consider submarine tectonic sources, fluid saturated marine sediment would require a different attenuation law. According to the new attenuation laws between distance and intensity in Italy calculated by Gomez Capera et al. (2019) for different Mw values, if we consider the distance between the Cittanova fault onland and the Ionian coastline (~20 km) where the slope failures activated, we obtain a level of intensity spanning 7.5–9.0 MCS degrees caused both by the February 1783 earthquake (Mw 7.1), and by other paleo-earthquakes sourced by this structure. During the 1783 earthquake, the villages facing the unstable continental margin along the Ionian coast experienced site intensities between 7–8 and 9–10 MCS. This level of intensity roughly matches a PGA of 150–400 cm/s^2 (0.15% g – 0.40% g) (i.e., Gomez Capera et al., 2019), well above the aforementioned stability threshold. On the other hand, considering that the distance between the Lakes fault and the Ionian coastline is ~30 km, a Mw 6.8 event triggered by this structure could induce effects of 7.0–8.0 MCS. The Mw 6.8 earthquake of June 1638 caused severe damage to the villages along the coast (around 8–9 MCS), which suggests a PGA of 250 cm/s^2 (0.26% g), which is above the stability threshold. In other words, we feel confident that the earthquakes sourced by the onshore Calabrian faults can really trigger turbidites along the Ionian unstable continental margin.

While historical and instrumental sources suggest that the Calabrian peninsula and the Tyrrhenian subduction zone hosted several large earthquakes during historical times, no medium-large earthquakes are reported by the seismic catalogues in the Ionian offshore region (Rovida et al., 2022). Strong shaking offshore Calabria can be caused by different faults: (1) crustal structures in the overriding plate; (2) transverse faults segmenting the continental margin; (3) megathrust earthquakes that originate at the

plate interface and/or splay faults (Polonia et al., 2011, 2012) (Fig. 1).

The new cores and, in particular, the correlation between seismo-turbidites and trench studies onshore, allow to speculate about the different tectonic sources and their activity. The upper plate events are mainly related to the Cittanova Fault (T1, 1783; T9-10, 3.5 ka; T16-17, 6.2 ka; and T19-T20, 10 ka) and Lakes fault (T2, 1638; T4, 7th century; T7-T8, 2.9 ka BP). PGA estimates suggest that these seismic events can trigger sediment remobilization in the offshore region. However, the number of seismo-turbidites is larger relative to the events reconstructed from trenches studies. All sedimentary events in historical times can be correlated with earthquakes onshore; however, when we go back in time, some of the turbidites cannot be correlated with known events onshore. This suggests that the record of fault activity onshore is not complete (e.g. other faults need to be considered) and/or that some of the seismo-turbidites are triggered by submarine faults.

Some of the sedimentary events that produced thick seismo-turbidites occurred 2–3 ka BP, 3.1–3.4 ka BP, 4.4–4.7 ka BP, 6.0–7.4 ka BP, 10 ka BP (T7, T10, T12, T17, T20). As these turbidites can be correlated in the different disconnected basins, these events are likely candidates for submarine fault activity, including the plate interface. Tomographic images suggest that central Calabria is the only region of the CA where the slab is still attached (Neri et al., 2009). However, its seismogenic behaviour is largely unknown, since subduction-type earthquakes were reported only in the Tyrrhenian Sea. This might be related to the lack of seismological marine studies and OBSs records (Sgroi et al., 2021a, 2021b). New seismological data from the western lobe of the subduction system that include data form a deep sea observatory, in fact, reveal the occurrence of a few thrust-type earthquakes in the accretionary wedge (Sgroi et al., 2021a). This might suggest a locked subduction interface in a complex tectonic setting involving the interplay between arc-orthogonal extension and plate convergence. Since the seismogenic layer of the subduction complex varies across strike from 20–30 km offshore Sicily to more than 70 km offshore southern Calabria (Sgroi et al., 2021a), we can speculate that, if the subduction thrust is locked and accumulating elastic strain, its rupture would involve a larger volume of lithosphere offshore Calabria, where it is thicker, increasing seismic hazard.

Since large earthquakes (magnitude $\geq$ 7.0) are rare, especially along slow-slipping plate boundaries such as the CA region, seismically triggered resedimented deposits have the potential to improve the seismological catalog extending the record of shaking events further back in time (Lu et al., 2020). T7, T10, T12, T17 and T20 are the more likely seismo-turbidites related to the subduction thrust activity because they can be correlated in the different disconnected basins and repeat every ~2–3 ka. Correlation between core stratigraphy and geophysical data can provide further information for longer time intervals (i.e. tens or hundreds of ka). The Chirp seismic profile collected during the recovery of core CALA-20 (Fig. 12a) show that the confined basin is filled by sedimentary units represented by high-amplitude seismic reflection possibly corresponding to the basal sandy part of turbidites and acoustically transparent units related to the homogenite part of the turbidites. Some of the acoustically transparent units are very thick and can be described as megaturbidites/homogenites. Three of these megabeds can be correlated to deposits in the Western Ionian Sea having similar ages (orange in Fig. 12b). Considering that the most recent of these megabeds (T5) is triggered by the CE365 megatsunami we propose that they represent Hellenic Arc seismic events that have produced trans-Mediterranean tsunamis and sediment remobilization in both lobes of the segmented CA subduction system (western and eastern lobes in Fig. 1). Megaturbidites of smaller thickness that cannot be correlated with deposits in the western Ionian Sea are interpreted as subduction-type earthquakes in the Eastern Lobe of the Calabrian Arc (T7, T10, T12, T17, T20, and other 9 events in the last 10 ka, green in Fig. 12a). Thinner turbidite beds (brown in Fig. 12a) are seismo-turbidites that might record the activity of crustal structures including faults onshore (about 15 events in the last 10 ka). If the megabeds from the CA represent larger earthquakes possibly related to subduction processes and activation of the subduction thrust, they repeat with long recurrence time (about 2–3 ka); this information should be taken into consideration for seismic hazard assessment.

7. Conclusions

The Calabrian Arc (CA) subduction system is one of the most seismically active region in the Mediterranean Sea. However, beyond sparse and uncertain reports from the 16th century, our knowledge of the regional seismicity starts only with the onset of the 17th century a time interval too short for a reliable seismic hazard assessment. In this study, we present an improved review of large-magnitude earthquakes obtained by integrating paleoseismological data onshore with the analysis of three gravity cores collected in disconnected sedimentary basins offshore Calabria. The close link between tectonic activity and co-seismic sedimentation is used to review major earthquakes during the Holocene and to infer seismic activity for a time interval long enough to include rare events such as those that possibly originate from the plate boundary interface.

We identified 20 turbidite beds (T1-T20) whose thickness varies between few centimetres to 1.5 m. Turbidite characterization was achieved through the analyses of geochemical and micropaleontological data that together with grain size help defining the composition and structure of distinct layers within the turbidite beds and sediment source. An abrupt increase in sand, Zr and Fe content and a sharp increase of density and diversity of benthic foraminifera mainly from the continental shelf areas (inner and outer shelf) characterize the turbidites. Two marker beds (Sapropel S1 and tephra Z-1 deposited during the Pompei eruption in 79 CE) combined with radiometric dating of hemipelagic layers allow to reconstruct turbidite emplacement time and interbasin turbidite correlation.

The deposition time window of the thickest turbidite T5 is in good correlation with the CE 365 Crete earthquake, confirming that the related megatsunami has generated turbidity currents on the opposite side of the Mediterranean basin. Far field events along the Hellenic Arc are capable of generating trans-Mediterranean tsunamis, increasing tsunami hazard. Above T5, four other turbidite beds were emplaced during the last millennia, and they are correlated with the Cittanova CE 1783, Lakes CE 1638, Rossano CE 951 and Lakes 7th century events. The age of older turbidites is less constrained in all cores. However, major events suggest emplacement time compatible with events that occurred at around 2.9 ka (Lakes fault), 3.5 ka (Cittanova fault), 6.2 ka (Cittanova fault) and 10 ka (Cittanova fault).

The number of seismo-turbidites is larger than the number of events reconstructed from trench studies onshore. All event deposits from historical times can be correlated with earthquakes onshore but when we go back in time, some of the turbidites cannot be correlated with known events. This suggests that the record of fault activity onshore is not complete (e.g. other faults need to be considered) and/or that some of the seismo-turbidites are triggered by submarine faults. Strong shaking offshore Calabria can be caused not only by earthquakes in the overriding plate but also by lithospheric faults segmenting the continental margin and by the subduction thrust.

While historical and instrumental sources suggest that the Calabrian peninsula and the Tyrrhenian subduction zone hosted sev-

eral large earthquakes during historical times, no medium-large earthquake is reported in the Ionian offshore region. This may indicate that subduction has already ceased or that the plate interface is locked and might produce large seismic events with long repeat time. Correlation between core stratigraphy and geophysical data provides further information for longer time intervals (i.e. 30–50 ka). Some of the resedimented units are very thick and can be described as megaturbidites/homogenites. Three of these megabeds can be correlated to deposits in the Western Ionian Sea with similar ages and may represent Hellenic Arc seismic events that produced trans-Mediterranean tsunamis. Megaturbidites of smaller thickness that cannot be correlated with deposits in the western Ionian Sea are interpreted as related to subduction processes in the eastern lobe of the CA where the slab is still attached. If this will be confirmed, the megabeds from the CA might represent larger earthquakes, possibly related to the subduction thrust activation that might repeat every 2–3 ka. Considering that the last megabed with these characteristics was deposited about 2.9 ka, this calls for a careful hazard assessment in this region.

CRediT authorship contribution statement

A. Polonia: Conceptualization, Data curation, Funding acquisition, Investigation, Methodology, Writing – original draft, Writing – review & editing. **R. Melis:** Data curation, Writing – original draft, Writing – review & editing. **P. Galli:** Data curation, Writing – original draft, Writing – review & editing. **E. Colizza:** Data curation, Writing – original draft, Writing – review & editing. **D. Insinga:** Data curation, Writing – original draft, Writing – review & editing. **L. Gasperini:** Data curation, Software, Funding acquisition, Writing – original draft, Writing – review & editing.

Declaration of Competing Interest

The authors declare that they have no known competing financial interests or personal relationships that could have appeared to influence the work reported in this paper.

Acknowledgments

We thank the CALAMARE scientific party and Urania shipboard party for their contribution in core collection. We are grateful to S. Miserocchi for acquisition of XRF data at ISMAR (Institute of Marine Sciences), to S. Romano for help in preparation of a previous version of Fig. 4 and to Laura Giordano for acquisition of tephra images. P. Petrosino and R. de' Gennaro are acknowledged for their assistance during SEM-EDS acquisition. This work has benefited from funding provided by the CNR for the R/V Urania shiptime. The Editorial Advisor Prof. M. Santosh, Associate Editor Prof. Masaki Yoshida, Marc De Batist and an anonymous reviewer are thanked for their constructive comments that helped improve this article.

Appendix A. Supplementary data

Supplementary data (**Supplementary Material 1** – Description of micropaleontological analyses. **Supplementary Material 2** – Optical microscope (left) and SEM (right) images to show lithology and leucite crystal occurrence in the two samples representative of the studied tephra. **Supplementary Material 3** – Age modelling results for core CALA-10: (a) Stratigraphic log, photograph and pelagic units with samples for radiometric datings of core CALA-10; (b) Deposition model built subtracting the thickness of the turbidites (instantaneous sedimentary events) from the total core; (c) Calibrated radiometric dates (2 σ) of the pelagic units using a ΔR_0; (d) age model built using the P_Sequence (a Bayesian model of deposition) implemented in the computer program OxCal 4.1 that assimilates sedimentation as a random process following a Poisson law (Bronk Ramsey, 2008). The regularity of sedimentation is determined by the k parameter (here k=3 reflects small variations in sedimentation rate as deduced from radiometric dating analysis. See section 5.5.4). The model finally calculates the age of each corrected depth corresponding to a turbidite and generates the 95.4% probability age ranges (2σ). **Supplementary Material 4** – Age modelling results for core CALA-20. Turbidite age distributions at 2σ are modelled from their stratigraphic depth of emplacement into the background sequence. The Oxcal software derives the sedimentation rate from a modelled time-depth curve for the dated hemipelagic sediments and finds mathematically a representative set of possible ages for each event point in the sedimentary sequence. **Supplementary Material 5** – Age modelling results for core CALA-10. Turbidite age distributions at 2σ are modelled from their stratigraphic depth of emplacement into the background sequence. The Oxcal software derives the sedimentation rate from a modelled time-depth curve for the dated hemipelagic sediments and finds mathematically a representative set of possible ages for each event point in the sedimentary sequence. **Supplementary Material 6 –** Comparison between turbidite emplacement time windows for core CALA-20 derived through Oxcal age modeling with k=3 and k=1.) to this article can be found online at https://doi.org/10.1016/j.gsf.2023.101612.

References

Bahrouni, N., Meghraoui, M., Başak Bayraktar, H., Lorito, S., Fawzi Zagrarni, M., Polonia, A., Bel Mabrouk, N., Kamoun, M., Khadraoui, A., Kamoun, F., 2022. Spread tsunami impact in East Tunisia contemporaneous of the CE 365 Crete earthquake. EGU22-9383, Vienna, 23th-27th May 2022.

Bortoluzzi, G., Polonia, A., Torelli, L., Artoni, A., Carlini, M., Carone, S., Carrara, G., Cuffaro, M., Bianco, F., D'Oriano, F., Ferrante, V., Gasperini, L., Ivaldi, R., Laterra, A., Ligi, M., Locritani, M., Muccini, F., Mussoni, P., Priore, F., Riminucci, F., Romano, S., Stanghellini, G., 2017. Styles and rates of deformation in the frontal accretionary wedge of the Calabrian Arc (Ionian Sea): controls exerted by the structure of the lower African plate. It. Jour. Geosc. 136, 347–364. https://doi.org/10.3301/IJG.2016.11.

Bronk Ramsey, C., 2008. Deposition models for chronological records. Quat. Sc. Rev. 27, 42–60. https://doi.org/10.1016/j.quascirev.2007.01.019.

Capozzi, R., Artoni, A., Torelli, L., Lorenzini, S., Oppo, D., Mussoni, P., Polonia, A., 2012. Neogene to Quaternary tectonics and mud diapirism in the Gulf of Squillace (Crotone-Spartivento Basin, Calabrian Arc, Italy). Mar. Petrol. Geol. 35, 219–234. https://doi.org/10.1016/j.marpetgeo.2012.01.007.

Casalbore, D., Chiocci, F.L., Scarascia, M.G., Tommasi, P., Sposato, A., 2011. Flash-flood hyperpycnal flows generating shallow-water landslides at Fiumara mouths in Western Messina Strait (Italy). Mar. Geophys. Res. 32, 257–271. https://doi.org/10.1007/s11001-011-9128-y.

Ceramicola, S., Fanucci, F., Corselli, C., Colizza, E., Morelli, D., Cova, A., Savini, A., Praeg, D., Zecchin, M., Caburlotto, A., Candoni, O., Civile, D., Coste, M., Cotterle, D., Critelli, S., Cuppari, A., Deponte, M., Dominici, R., Forlin, E., Gordini, E., Tessarolo, C., Marchese, F., Muto, F., Palamara, S., Ramella, R., Facchin, L., Romeo, R., 2021. Tavola 8. Calabria Ionica, 175-195. In: Chiocci F.L., et al. (2021) Atlante dei lineamenti di pericolosità geologica dei mari italiani- Risultati del progetto MaGIC. CNR edizioni, Roma (in Italian).

Chester, R., 2000. Marine Geochemistry. 2 editions. Unwin Hyman, London, Wiley-Blackwell, 520 pp. https://doi.org/10.1007/978-94-010-9488-7.

Cotecchia, V., Guerricchio, A., Melidoro, G., 1986. The geomorphogenetic crisis triggered by the 1783 earthquake in Calabria (southern Italy). In: Proceed. of the Int. Symp. on "Engineering Geology Problems in Seismic Areas", vol. 6, Cotecchia V. (Ed)., 245–304, Istituto di Geologia applicata e Geotecnica, Università degli studi di Bari, Bari, Italy.

Cuppari, A., Colizza, E., Fanucci, F., Morelli, D., 2004. Morphology and evolution of the Siderno and Bovalino canyons (Ionian Margin): Relation with tectonics of Calabrian Arc (Calabrian Ionian Margin). Quat. Nova 8, 29–44.

D'Agostino, N., Avallone, A., Cheloni, D., D'Anastasio, E., Mantenuto, S., Selvaggi, G., 2008. Active tectonics of the Adriatic region from GPS and earthquake slip vectors. J. Geophys. Res. 113, B12413. https://doi.org/10.1029/2008JB005860.

Dan, G., Sultan, N., Savoye, B., Deverchere, J., Yelles, K., 2009. Quantifying the role of sandy–silty sediments in generating slope failures during earthquakes: example from the Algerian margin. Intern. J. Earth Sci. 98 (4), 769–789. https://doi.org/10.1007/s00531-008-0373-5.

De Lange, G.J., Thomson, J., Reitz, A., Slomp, C.P., Principato, M.S., Erba, E., Corselli, C., 2008. Synchronous basin-wide formation and redox-controlled preservation of

a Mediterranean sapropel. Nat. Geosci. 1, 606–610. https://doi.org/10.1038/ngeo283.
Doronzo, D., Di Vito, M.A., Arienzo, I., Bini, M., Calusi, B., Cerminara, M., Corradini, S., de Vita, S., Giaccio, B., Gurioli, L., Mannella, G., Ricciardi, G.P., Rucco, I., Sparice, D., Todesco, M., Trasatti, E., Zanchetta, G., 2022. The 79 CE eruption of Vesuvius: A lesson from the past and the need of a multidisciplinary approach for developments in volcanology. Earth Sci. Rev. 231, 104072.
Douglas, J., 2003. Earthquake ground motion estimation using strong-motion records: a review of equations for the estimation of peak ground acceleration and response spectral ordinates. Earth Sci. Rev. 61 (1–2), 43–104. https://doi.org/10.1016/S0012-8252(02)00112-5.
ENEL, 1986. I Terremoti Calabresi del 1783. ENEL, Bologna (in Italian).
Faccenna, C., Funiciello, F., Civetta, L., D'Antonio, M., Moroni, M., Piromallo, C., 2007. Slab disruption, mantle circulation, and the opening of the Tyrrhenian basins. In: Beccaluva, L., Bianchini, G., Wilson, M. (Eds.), Cenozoic Volcanism in the Mediterranean Area. Geol. Soc. Am. Sp. Pap., 41, 153-169. https://doi.org/10.1130/2007.2418(08).
Ferreli, L., Michetti, A.M., Serva, L., Vittori, E., 2002. Stratigraphic evidence of coseismic faulting and aseismic fault creep from exploratory trenches at Mt. Etna volcano (Sicily, Italy). In: Ettensohn, F.R., Rast, N., Brett, C.E. (Eds.), Ancient Seismites, Boulder: Colorado. Geol. Soc. Am. Sp. Pap, 359, 49-62.
Folk, R.L., Ward, W.C., 1957. Brazos River bar: A study in the significance of grain size parameters. Jour. Sedim. Res. 27, 3–26.
Frezza, V., Carboni, M.G., 2009. Distribution of recent foraminiferal assemblages near the Ombrone River mouth (Northern Tyrrhenian Sea, Italy). Rev. Micropal 52 (1), 43–66. https://doi.org/10.1016/j.revmic.2007.08.007.
Friedman, G.M., Sanders, J.E., 1978. Principles of Sedimentology. John Wiley, New York, p. 792.
Galli, P., 2020. Recurrence times of central-southern Apennine faults (Italy): hints from paleoseismology. Terra Nova 32 (6), 399–407. https://doi.org/10.1111/ter.12470.
Galli, P., Bosi, V., 2002. Paleoseismology along the Cittanova fault: Implications for seismotectonics and earthquake recurrence in Calabria (southern Italy). Jour. Geophys. Res. 107 (B3), ETG 1-1-ETG 1-19. https://doi.org/10.1029/2001JB000234.
Galli, P., Bosi, V., 2003. Catastrophic 1638 earthquakes in Calabria (southern Italy): New insight from paleoseismological investigation. Jour. Geophys. Res. 108 (B1), ETG 1-1-ETG 1-20. .
Galli, P., Molin, D., 2007. Il terremoto del 1905 della Calabria meridionale. Studio analitico degli effetti ed ipotesi sismogenetiche, http://ilmiolibro.kataweb.it/libro.asp?id=14201, Gruppo Editoriale L'Espresso, Roma, 110 pp.
Galli, P., Scionti, V., 2006. Two unknown M>6 historical earthquakes revealed by paleoseismological and archival researches in eastern Calabria (southern Italy). Seismotectonic implication. Terra Nova 18 (1), 44–49. https://doi.org/10.1111/j.1365-3121.2005.00658.x.
Galli, P., Scionti, V., Spina, V., 2007. New paleoseismic data from the Lakes and Serre faults (Calabria, southern Italy). Seismotectonic implication. Boll. Soc. Geol. Ital. 126, 347–364.
Galli, P., Galadini, F., Pantosti, D., 2008. Twenty years of paleoseismology in Italy. Earth Sc. Rev. 88, 89–117. https://doi.org/10.1016/j.earscirev.2008.01.001.
Galli, P., Peronace, E., 2015. Low slip rates and multi-millennial return times for *Mw* 7 earthquake faults in southern Calabria (Italy). Geoph. Res. Lett. 13, 5258–5265. https://doi.org/10.1002/2015GL064062.
Galli, P., Spina, V., Ilardo, I., Naso, G., 2010. Evidence of active tectonics in southern Italy: the Rossano Fault (Calabria). In: Guarnieri, P. (Ed.), Recent Progress on Earthquake Geology. Nova Scientific Publisher Inc., New York, pp. 49–78.
Gasperini, L., Stanghellini, G., 2009. SEISPRHO: An interactive computer program for processing and interpretation of high-resolution seismic reflection profiles. Comput. & Geosc. 35, 1497–1507. https://doi.org/10.1016/j.cageo.2008.04.014.
GdL, 2004. Redazione della mappa di pericolosità simsica prevista dall'Ordinanza PCM 3274, 20/03/03, Rapporto Conclusivo per il DPC. INGV, 65 pp.
Goldfinger, C., 2011. Submarine paleoseismology based on turbidite records. Annu. Rev. Marine. Sci. 3, 35–66. https://doi.org/10.1146/annurev-marine-120709-142852.
Goldfinger, C., Nelson, C.H., Morey, A.E., Johnson, J.E., Patton, J.R., Karabanov, E., Gutiérrez-Pastor, J., Eriksson, A.T., Gràcia, E., Dunhill, G., Enkin, R.J., Dallimore, A., Vallier, T., 2012, Turbidite event history—Methods and implications for Holocene paleoseismicity of the Cascadia subduction zone. U.S. Geological Survey Professional Paper 1661–F, 170 pp. https://pubs.usgs.gov/pp/pp1661f/.
Gomez Capera, A.A., Santulin, M., Massa, M., Locati, M., 2019. Definizione di una nuova IPE per il territorio italiano in funzione di Mw sulla base di CPTI15 e DBMI15. INGV, MPS19 - Rapporto Finale. Centro di Pericolosità Sismica, 12 pp. in Italian.
Govers, R., Wortel, M.J.R., 2005. Lithosphere tearing at STEP faults: Response to edges of subduction zones. Earth Planet. Sci. Lett. 236, 505–523. https://doi.org/10.1016/j.epsl.2005.03.022.
Gutierrez-Pastor, J., Nelson, C.H., Goldfinger, C., Johnson, J.E., Escutia, C., Eriksson, A., Morey, A.E., the Shipboard Scientific Party, 2009. Earthquake Control of Holocene Turbidite Frequency Confirmed by Hemipelagic Sedimentation Chronology on the Cascadia and Northern California Active Continental Margins. External Controls on Deep-Water Depositional Systems, SEPM Sp. Publ. 92, SEPM (Society for Sedimentary Geology), 179 – 197.
Harders, R., Kutterolf, S., Hensen, C., Moerz, T., Brueckmann, W., 2010. Tephra layers: A controlling factor on submarine translational sliding? Geoch. Geophys. Geosyst. 11 (5), Q05S23. https://doi.org/10.1029/2009GC002844.
Heaton, T., Köhler, P., Butzin, M., Bard, E., Reimer, R., Austin, W., Bronk Ramsey, C., Grootes, P.M., Hughen, K.A., Kromer, B., Reimer, P.J., Adkins, J., Burke, A., Cook, M.S., Olsen, J., Skinner, L., 2020. Marine20—The Marine Radiocarbon Age Calibration Curve (0–55,000 cal BP). Radiocarbon 62 (4), 779–820. https://doi.org/10.1017/RDC.2020.68.
Insinga, D.D., Petrosino, P., Alberico, I., de Lange, G.J., Lubritto, C., Molisso, F., Sacchi, M., Sulpizio, R., Wu, J., Lirer, F., 2020. The Late Holocene tephra record of the central Mediterranean Sea: Mapping occurrences and new potential isochrons for the 4.4-2.0 ka time interval. J. Quat. Sci. 35 (1–2), 213–231. https://doi.org/10.1002/jqs.3154.
Jorissen, F.J., 1988. Benthic foraminifera from the Adriatic Sea: principles of phenotypic variation. Utrecht Micropal. Bull. 37, 1–174.
Keefer, D.K., 1984. Landslides caused by earthquakes. Geol. Soc. Am. Bull. 95, 406–421.
Keller, J., Ryan, W.B.F., Ninkovich, D., Altherr, R., 1978. Explosive volcanic activity in the Mediterranean over the past 200,000 yr as recorded in deep-sea sediments. Geol. Soc. Am. Bull. 89, 591–604.
Le Maitre, R.W., 2005. Igneous rocks. A classification and glossary of terms. Recommendations of the International Union of Geological Sciences, Subcommission on the Systematics of Igneous Rocks. Cambridge University Press, Cambridge.
Lirer, L., Pescatore, T., Booth, B., Walker, G.P.L., 1973. Two Plinian Pumice-Fall deposits from Somma-Vesuvius. Italy. Geol. Soc. Am. Bull 84, 759–772.
Lorito, S., Tiberti, M.M., Basili, R., Piatanesi, A., Valensise, G., 2008. Earthquake-generated tsunamis in the Mediterranean Sea: Scenarios of potential threats to Southern Italy. J. Geophys. Res. 113, B01301. https://doi.org/10.1029/2007JB004943.
Lu, Y., Wetzler, N., Waldmann, N., Agnon, A., Biasi, G.P., Marco, S., 2020. A 220,000-year-long continuous large earthquake record on a slow-slipping plate boundary. Sci. Adv. 6, eaba4170.
Maesano, F.E., Tiberti, M.M., Basili, R., 2017. The Calabrian Arc: three-dimensional modelling of the subduction interface. Sci. Rep. 7, 8887 https://doi.org/10.1038/s41598-017-09074-8.
Margottini, C., Ambraseys, N.N., Screpanti, A., 1993. La magnitudo dei terremoti italiani del XX secolo. ENEA, Roma, p. 57.
McHugh, C.M.G., Seeber, L., Cormier, M.-H., Dutton, J., Çagatay, M.N., Polonia, A., Ryan, W.B.F., Görür, N., 2006. Submarine earthquake geology along the North Anatolian Fault in the Marmara Sea, Turkey: A model for transform basin sedimentation. Earth Planet. Sc. Lett. 248, 661–684. https://doi.org/10.1016/j.epsl.2006.05.038.
Melluso, L., Scarpati, C., Zanetti, A., Sparice, D., de' Gennaro, R.,, 2022. The petrology and geochemistry of zoned, phonolitic Plinian and sub-Plinian eruptions of Somma-Vesuvius, Italy: role of accessory phase removal, independently filled magma reservoirs with time, and transition from slightly to highly silica undersaturated series in an ultrapotassic stratovolcano. Lithos 430–431, 106854.
Meunier, P., Hovius, N., Haines, A.J., 2007. Regional patterns of earthquake-triggered landslides and their relation to ground motion. Geophys. Res. Lett. 34 (20), L20408. https://doi.org/10.1029/2007GL031337.
Michelini, A., Lomax, A., Nardi, A., Rossi, A., 2006. La localizzazione del terremoto della Calabria dell'8 settembre 1905 da dati strumentali. In Guerra e Savaglio, 225–240. in Italian.
Miglietta, M.M., Laviola, S., Malvaldi, A., Conte, D., Levizzani, V., Price, C., 2013. Analysis of tropical-like cyclones over the Mediterranean Sea through a combined modeling and satellite approach. Geophys. Res. Lett. 40, 2400–2405. https://doi.org/10.1002/grl.50432.
Moernaut, J., Van Daele, M., Heirman, K., Fontijn, K., Strasser, M., Pino, M., Urrutia, R., De Batist, M., 2014. Lacustrine turbidites as a tool for quantitative earthquake reconstruction: new evidence for a variable rupture mode in South-Central Chile. J. Geophys. Res. – Solid Earth 119 (3), 1607–1633.
Mottershead, D.N., Bray, M.J., Soar, P.J., 2018. Tsunami landfalls in the Maltese archipelago: reconciling the historical record with geomorphological evidence. Geochem. Soc. Spec. Publ. 456, 127–141.
Murray, J.W., 2006. Ecology and Applications of Benthic Foraminifera. Cambridge University Press, New York, p. 426.
Nakajima, T., Kanai, Y., 2000. Sedimentary features of seismoturbidites triggered by the 1983 and older historical earthquakes in the eastern margin of the Japan Sea. Sedim. Geol. 135, 1–19. https://doi.org/10.1016/S0037-0738(00)00059-2.
Nardelli, M.P., Jorissen, F.J., Pusceddu, A., Morigi, C., Dell'Anno, A., Danovaro, R., de Stigter, H.C., Negri, A., 2010. Living benthic foraminiferal assemblages along a latitudinal transect at 1000 m depth off the Portuguese margin. Micropaleontology 56, 323–344. https://doi.org/10.2307/40959487.
Nelson, C.H., Gutiérrez Pastor, J., Goldfinger, C., Escutia, C., 2012. Great earthquakes along the Western United States continental margin: implications for hazards, stratigraphy and turbidite lithology. Nat. Hazards Earth Syst. Sci. 12, 3191–3208. https://doi.org/10.5194/nhess-12-3191-2012.
Neri, G., Orecchio, B., Totaro, C., Falcone, G., Presti, D., 2009. Subduction beneath southern Italy close the ending: Results from seismic tomography. Seismol. Res. Lett. 80, 63–70. https://doi.org/10.1785/gssrl.80.1.63.
Neri, G., Marotta, A.M., Orecchio, B., Presti, D., Totaro, C., Barzaghi, R., Borghi, A., 2012. How lithospheric subduction changes along the Calabrian Arc in southern Italy: geophysical evidences. Int. J. Earth Sci. 101 (7), 1949–1969. https://doi.org/10.1007/s00531-012-0762-7.
Panieri, G., Polonia, A., Lucchi, R.G., Zironi, S., Capotondi, L., Negri, A., Torelli, L., 2013. Mud volcanoes along the inner deformation front of the Calabrian Arc

accretionary wedge (Ionian Sea). Mar. Geol. 336, 84–98. https://doi.org/10.1016/j.margeo.2012.11.003.
Patton, J.R., Goldfinger, C., Morey, A.E., Ikehara, K., Romsos, C., Stoner, J., Djadjadihardja, Y., Udrekh, Ardhyastut, S., Zulkarnaen Gaffar, E., Vizcaino, A., 2015. A 6600-year earthquake history in the region of the 2004 Sumatra-Andaman subduction zone earthquake. Geosphere 11 (9), 1–63. https://doi.org/10.1130/GES01066.1.
Polonia, A., Torelli, L., Mussoni, P., Gasperini, L., Artoni, A., Klaeschen, D., 2011. The Calabrian Arc Subduction Complex in the Ionian Sea: Regional architecture, active deformation and seismic hazard. Tectonics 30, TC5018. https://doi.org/10.1029/2010TC002821.
Polonia, A., Torelli, L., Gasperini, L., Mussoni, P., 2012. Active faults and historical earthquakes in the Ionian Sea. Nat. Hazards Earth Syst. Sci. 12, 2311–2328. https://doi.org/10.5194/nhess-12-2311-2012.
Polonia, A., Panieri, G.L., Gasperini, G., Gasparotto, L.G., Bellucci, L., Torelli, L., 2013a. Turbidite paleoseismology in the Calabrian Arc subduction complex (Ionian Sea). Geochem. Geophys. Geosyst. 14, 112–140. https://doi.org/10.1029/2012GC004402.
Polonia, A., Bonatti, E., Camerlenghi, A., Lucchi, R.G., Panieri, G., Gasperini, L., 2013b. Mediterranean megaturbidite triggered by the AD 365 Crete earthquake and tsunami. Sci. Rep. 3, 1285. https://doi.org/10.1038/srep01285.
Polonia, A., Romano, S., Çağatay, N.M., Capotondi, L., Gasparotto, G., Gasperini, L., Panieri, G., Torelli, L., 2015. Is repetitive slumping during sapropel S1 related to paleo-earthquakes? Mar. Geol. 361, 41–52. https://doi.org/10.1016/j.margeo.2015.01.001.
Polonia, A., Vaiani, C.S., De Lange, G., 2016a. Did the AD 365 Crete earthquake/tsunami trigger synchronous giant turbidity currents in the Mediterranean Sea? Geology 44, 191–194. https://doi.org/10.1130/G37486.1.
Polonia, A., Torelli, L., Artoni, A., Carlini, M., Faccenna, C., Ferranti, L., Gasperini, L., Govers, R., Klaeschen, D., Monaco, C., Neri, G., Nijholt, N., Orecchio, B., Wortel, R., 2016b. The Ionian and Alfeo-Etna fault zones: New segments of an evolving plate boundary in the central Mediterranean Sea? Tectonophysics 675, 69–90. https://doi.org/10.1016/j.tecto.2016.03.016.
Polonia, A., Bonetti, C., Bonetti, J., Çağatay, M.N., Gallerani, A., Gasperini, L., Nelson, C.H., Romano, S., 2021a. Deciphering co-seismic sedimentary processes in the Mediterranean Sea using elemental, organic carbon and isotopic data. Geochem. Geophys. Geosyst. 22(7), e2020GC009446. https://doi.org/10.1029/2020GC009446.
Polonia, A., Brancolini, G., Torelli, L., Vera, E., 1999. Structural variability at the active continental margin off Southernmost Chile. J. Geodyn. 27, 289–307.
Polonia, A., Nelson, C.H., Romano, S., Vaiani, S.C., Colizza, E., Gasparotto, G., Gasperini, L., 2017a. A depositional model for seismo-turbidites in confined basins based onIonian Sea deposits. Mar. Geol. 384, 177–198. https://doi.org/10.1016/j.margeo.2016.05.010.
Polonia, A., Torelli, L., Gasperini, L., Cocchi, L., Muccini, F., Bonatti, E., Hensen, C., Schmidt, M., Romano, S., Artoni, A., Carlini, M., 2017b. Lower plate serpentinite diapirism in the Calabrian Arc subduction complex. Nature Commun. 8 (1), 2172. https://doi.org/10.1038/s41467-017-02273-x.
Polonia, A., Albertazzi, S., Bellucci, L.G., Bonetti, C., Giorgetti, G., Giuliani, S., López Correa, M., Mayr, C., Peruzza, L., Stanghellini, G., Gasperini, L., 2021b. Decoding a complex record of anthropogenic and natural impacts in the Lake of Cavazzo sediments, NE Italy. Sci. Tot. Environ. 787, 147659. https://doi.org/10.1016/j.scitotenv.2021.147659.
Polonia, A., Nelson, C.H., Vaiani, S.C., Colizza, E., Gasparotto, G., Giorgetti, G., Bonetti, C., Gasperini, L., 2022. Recognizing megatsunamis in Mediterranean deep sea sediments based on the massive deposits of the 365 CE Crete event. Sci. Rep. 12 (1), 1–20 https://www.nature.com/articles/s41598-022-09058-3.
Pouderoux, H., Lamarche, G., Proust, J.-N., 2012. Building an 18 000-year-long paleoearthquake record from detailed deep-sea turbidite characterisation in Poverty Bay, New Zealand. Nat. Hazards Earth Syst. Sci. 12, 2077–2101. https://doi.org/10.5194/nhess-12-2077-2012.
Puig, P., Ogston, A.S., Mullenbach, B.L., Nittrouer, C.A., Parsons, J.D., Sternberg, R.W., 2004. Storm-induced sediment gravity flows at the head of the Eel submarine canyon, northern California margin. J. Geophys. Res. 109, C03019. https://doi.org/10.1029/2003JC001918.
Pujol, C., Vergnaud Grazzini, C., 1995. Distribution patterns of live planktic foraminifers as related to regional hydrography and productive systems of the Mediterranean Sea. Mar. Micropal. 25 (2–3), 187–217. https://doi.org/10.1016/0377-8398(95)00002-I.
Rossi, S., Sartori, R., 1981. A seismic reflection study of the external Calabrian arc in the northern Ionian Sea (Eastern Mediterranean). Mar. Geophys. Res. 4, 403–426.
Rovida, A., Locati, M., Camassi, R., Lolli, B., Gasperini, P., Antonucci, A., 2022. Catalogo Parametrico dei Terremoti Italiani (CPTI15), versione 4.0. Istituto Nazionale di Geofisica e Vulcanologia (INGV). https://doi.org/10.13127/CPTI/CPTI15.4.
Salama, A., Meghraoui, M., El Gabry, M., Maouche, S., Hussein, M.H., Korrat, I., 2018. Paleotsunami deposits along the coast of Egypt correlate with historical earthquake records of eastern Mediterranean. Nat. Hazards Earth Syst. Sci. 18, 2203–2219. https://doi.org/10.5194/nhess-18-2203-2018.
Sammartini, M., Camerlenghi, A., Budillon, F., Insinga, D.D., Zgur, F., Conforti, A., Iorio, M., Romeo, M., Tonielli, R., 2019. Open-slope, translational submarine landslide in a tectonically active volcanic continental margin (Licosa submarine landslide, southern Tyrrhenian Sea). In: Lintern, D.G., Mosher, D.C., Moscardelli, L.G., Bobrowsky, P.T., Campbell, C., Chaytor, J.D., Clague, J.J., Georgiopoluou, A., Lajeunesse, P., Normandeau, A., Piper, D.J.W., Scherwath, M., Stacey, C., Turmel, D. (Eds), Subaqueous Mass Movements. Geological Society, London, Sp. Publ., 477, 133–150.
San Pedro, L., Babonneau, N., Gutscher, M.-A., Cattaneo, A., 2017. Origin and chronology of the Augias deposit in the Ionian Sea (Central Mediterranean Sea), based on new regional sedimentological data. Mar. Geol. 384 (10), 199–213. https://doi.org/10.1016/j.margeo.2016.05.005.
Santacroce, R., Cioni, R., Marianelli, P., Sbrana, A., Sulpizio, R., Zanchetta, G., Donahue, D.J., Joron, J.L., 2008. Age and whole rock–glass compositions of proximal pyroclastics from the major explosive eruptions of Somma-Vesuvius: A review as a tool for distal tephrostratigraphy. J. Volcan. Geoth. Res. 177, 1–18. https://doi.org/10.1016/j.jvolgeores.2008.06.009.
Schambach, L., Grilli, S.T., Tappin, D.R., Gangemi, M.D., Barbaro, G., 2020. New simulations and understanding of the 1908 Messina tsunami for a dual seismic and deep submarine mass failure source. Mar. Geol. 421, 106093. https://doi.org/10.1016/j.margeo.2019.106093.
Scionti, V., Galli, P., 2004. Ricerche sulla sismicità storica della Calabria tra XV e XVIII secolo. Rapporto Tecnico DPC/USSN 94.
Scionti, V., Galli, P., Chiodo, G., 2006. The Calabrian seismicity during the Viceroyalty of Naples: Sources silence or silent sources? The case of the strong 1744 earthquake. Boll. Geof. Teor. Appl. 47, 53–72.
Selvaggi, G., Chiarabba, C., 1995. Seismicity and P-wave velocity image of the Southern Tyrrhenian Subduction Zone. Geophys. J. Int. 121 (3), 818–826.
Sgarrella, F., Moncharmont Zei, M., 1993. Benthic foraminifera of the Gulf of Naples (Italy): systematics and autoecology. Boll. Soc. Paleont. It. 32 (2), 145–264.
Sgroi, T., Polonia, A., Barberi, G., Billi, A., Gasperini, L., 2021a. New seismological data from the Calabrian Arc reveal arc-orthogonal extension across the subduction zone. Sci. Rep. 11, 473. https://doi.org/10.1038/s41598-020-79719-8.
Sgroi, T., Polonia, A., Beranzoli, L., Billi, A., Bosman, A., Costanza, A., Cuffaro, M., D'Anna, G., De Caro, M., Di Nezza, M., Fertitta, G., Frugoni, F., Gasperini, L., Monna, S., Montuori, C., Petracchini, L., Petricca, P., Pinzi, S., Ursino, A., Doglioni, C., 2021b. One year of seismicity recorded through ocean bottom seismometers illuminates active tectonic structures in the Ionian Sea (Central Mediterranean). Front. Earth Sci. 9, 661311. https://doi.org/10.3389/feart.2021.661311.
Shaw, B., Ambraseys, N.N., England, P.C., Floyd, M.A., Gorman, G.J., Higham, T.F.G., Jackson, J.A., Nocquet, J.-M., Pain, C.C., Piggott, M.D., 2008. Eastern Mediterranean tectonics and tsunami hazard inferred from the AD 365 earthquake. Nat. Geosc. 1, 268–276. https://doi.org/10.1038/ngeo151.
Smedile, A., De Martini, P.M., Pantosti, D., Bellucci, L., Del Carlo, P., Gasperini, L., Pirrotta, C., Polonia, A., Boschi, E., 2011. Possible tsunamis signatures from an integrated study in the Augusta Bay offshore (Eastern Sicily-Italy). Mar. Geol. 281, 1–13. https://doi.org/10.1016/j.margeo.2011.01.002.
Strasser, M., Stegmann, S., Bussmann, F., Anselmetti, F.S., Rick, B., Kopf, A., 2007. Quantifying subaqueous slope stability during seismic shaking: Lake Lucerne as model for ocean margins. Mar. Geol. 240, 77–97. https://doi.org/10.1016/j.margeo.2007.02.016.
Strasser, M., Moneke, K., Schnellmann, M., Anselmetti, F.S., 2013. Lake sediments as natural seismographs: A compiled record of Late Quaternary earthquakes in Central Switzerland and its implication for Alpine deformation. Sedimentology 60, 319–341. https://doi.org/10.1111/sed.12003.
Stuiver, M., Reimer, P.J., 1993. Extended 14C data base and revised CALIB 3.0 ^{14}C age calibration program. Radiocarbon 35, 215–230.
Tinti, S., Armigliato, A., Pagnoni, G., Zaniboni, F., 2005. Scenarios of giant tsunamis of tectonic origin in the Mediterranean. Paper No. 464, ISET Jour. Earthquake Technol. 42(4), 171–188.
Tinti, S., Maramai, A., Graziani, L., 2004. The new catalogue of the Italian tsunamis. Nat. Hazards 33, 439–465. https://doi.org/10.1023/B:NHAZ.0000048469.51059.65.
Totaro, F., Insinga, D.D., Lirer, F., Margaritelli, G., Català i Caparrós, A., de la Fuente, M., Petrosino, P., 2022. The Late Pleistocene to Holocene tephra record of ND14Q site (southern Adriatic Sea): traceability and preservation of Neapolitan explosive products in the marine realm. J. Volcanol. Geoth. Res. 423, 107461.
Van Daele, M., Cnudde, V., Duyck, P., Pino, M., Urria, R., De Batist, M., 2014. Multidirectional, synchronously-triggered seismo-turbidites and debrites revealed by X-ray computed tomography (CT). Sedimentology 61 (4), 861–880. https://doi.org/10.1111/sed.12070.
Van Daele, M., Versteeg, W., Pino, M., Urrutia, R., De Batist, M., 2013. Widespread deformation of basin-plain sediments in Aysén fjord (Chile) due to impact by earthquake-triggered, onshore-generated mass movements. Mar. Geol. 337, 67–79. https://doi.org/10.1016/j.margeo.2013.01.006.
Van Daele, M., Meyer, I., Moernaut, J., Dedecker, S., Verschuren, D., De Batist, M., 2017. A revised classification and terminology for stacked and amalgamated turbidites in environments dominated by (hemi)pelagic sedimentation. Sedim. Geol. 357, 72–82.
van Hinsbergen, D.J.J., Kouwenhoven, T.J., van der Zwaan, G.J., 2005. Paleobathymetry in the backstripping procedure: Correction for oxygenation effects on depth estimates. Palaeogeogr. Palaeocl. Palaeoecol. 221 (3–4), 245–265. https://doi.org/10.1016/j.palaeo.2005.02.013.
Vannucci, G., Gasperini, P., 2004. The new release of the database of earthquake mechanisms of the Mediterranean Area (EMMA version 2). Ann. Geophys. 47 (S1), 307–334. doi:10.4401/ag-3277.
Wortel, M.J.R., Spakman, W., 2000. Subduction and slab detachment in the Mediterranean-Carpathian Region. Science 290, 1910–1917. https://doi.org/10.1126/science.290.5498.1910.